Table 1. Prognostic significance of actinin-4 expression in 173 cases of invasive ductal carcinoma of the pancreas

	Univariate analysis*			Multivariate analysis*		
	Hazard ratio	95% Confidence interval	P †	Hazard ratio	95% Confidence interval	P †
Age (y)						
<65/≥65	1.18	0.85-1.65	0.321584			
Gender						
Male/female	1.12	0.80-1.57	0.515322			
UICC stage ‡						
I-II/III-IV	2.59	1.31-5.12	0.006191	1.35	0.59-3.08	0.471917
Extent of primary tumor ‡						
T_{1-2}/T_{3-4}	1.81	1.16-2.82	0.008528	0.86	0.52-1.44	0.572695
Lymph node metastasis ‡						
N_0/N_1	2.73	1.82-4.08	0.000001	1.96	1.20-3.19	0.007271
Distant metastasis ‡						
M_0/M_1	2.40	1.68-3.44	0.000002	1.73	1.18-2.54	0.005023
Lymphatic invasion§						
ly0/ly1-3	2.06	1.44-2.95	0.000076	1.54	1.03-2.28	0.033537
Intrapancreatic nerve invasion§						
ne0/ne1-3	1.26	0.89-1.77	0.189521			
Macroscopic type§						
Nodular/infiltrative	1.28	0.91-1.80	0.162522			
Cancer-stroma relationship§						
Medullary and intermediate/scirrhous	1.14	0.81-1.60	0.458187			
Expression of actinin-4						
Positive/negative	2.27	1.57-3.27	0.000012	2.33	1.61-3.39	0.000009

*Univariate and multivariate analyses with Cox proportional hazards model.
† $P < 0.01$ was considered statistically significant.
‡ Based on the International Union Against Cancer tumor-node-metastasis classification (6th edition).
§ Based on the Japan Pancreas Society's classification of pancreatic carcinoma (2nd English edition).

progress into invasive tumors, suggesting that additional genetic events must occur for the development of fully malignant pancreatic tumors (10). Recurrent amplification of the chromosome locus 19q13.1-2 has been reported in pancreatic cancer cell lines and primary pancreatic cancers (11-13). Earlier studies indicated that the *AKT2* gene was the target of amplification, but *AKT2* was not always overexpressed in pancreatic cancer cell lines with gene amplification (14, 15), and its down-regulation by small interfering RNA did not significantly affect cell viability (16), leaving the precise target gene(s) of the 19q13.1-2 amplicon undetermined.

The histopathology of pancreatic cancer invariably reveals massive infiltration of small cancer nests lacking a glandular structure. This invasive growth pattern seems to be an intrinsic feature of pancreatic carcinogenesis and might reflect a specific underlying genetic alteration. The *ACTN4* gene that encodes actinin-4 has been mapped to chromosome 19q13[7] in the vicinity of the amplification described above (13). On the basis of these histopathologic and genetic observations, we hypothesized that the *ACTN4* gene might be a target of the 19q13.1-2 amplification and may play a significant role in the invasive growth of pancreatic ductal carcinoma. Because gene amplification is known to activate several oncogenes by increasing their expression levels (17), we first investigated the expression of actinin-4 in clinical samples of pancreatic cancer in order to assess the clinical relevance of any expression changes.

Patients and Methods

Immunohistochemistry. Immunohistochemical analysis was done on tissue specimens from 173 patients with pancreatic ductal carcinoma who had undergone surgical resection between 1990 and 2003 at the National Cancer Center Hospital (Tokyo, Japan) without any prior therapy. The tumors were staged according to the International Union Against Cancer (UICC) tumor-node-metastasis classification (18). Other pathologic variables (macroscopic type, lymphatic invasion, intrapancreatic nerve invasion, and cancer-stroma relationship; Table 1) were categorized according to the Japan Pancreas Society's classification of pancreatic carcinoma (19). The mean follow-up period was 25.7 months (ranging from 1 to 171 months). The protocol of this study was reviewed and approved by the institutional ethics committee.

Formalin-fixed paraffin-embedded tissue sections (5 μm thick) were stained by the immunoperoxidase method with avidin-biotin complex as described previously (20). We confirmed the absence of nonspecific staining by omitting the first antibody. Immunohistochemical results were judged by three investigators (S. Kikuchi, K. Honda, and N. Hiraoka) who were unaware of the clinical data.

Cell lines. All pancreatic cancer cell lines used in this study (BxPC3, AsPc-1, Mpanc96, Panc-1, MIA-PACA2, CFPAC-1, Capan-1, Capan-2, HPAC, Su86.86, and MIA-PACA) were obtained from the American Type Culture Collection.

Antibodies. Anti-actinin-4 rabbit polyclonal (Ab-2) and anti-E-cadherin mouse monoclonal (HECD-1) antibodies were generated as described previously (6, 21). Anti-pan AKT rabbit polyclonal

[7] http://www.ncbi.nlm.nih.gov/mapview/

antibody was purchased from Cell Signaling Technology. Anti-AKT2 mouse monoclonal antibody (F-7) was purchased from Santa Cruz Biotechnology. Anti-β-actin mouse monoclonal antibody (AC-15) was purchased from Abcam. Anti-Ki67 antigen mouse monoclonal antibody (MiB-1) was purchased from Dako.

Western blot analysis. Cells were extracted with lysis buffer [10 mmol/L HEPES (pH 7.4), 150 mmol/L NaCl, 1 mmol/L EDTA, 1% Triton X-100, 1% NP40, and 1 mg/mL NaN_3] containing a protease inhibitor cocktail (Sigma-Aldrich) on ice for 30 min. Cell lysates were separated by SDS-PAGE and transferred to Immobilon-P membranes (Millipore). After incubation with primary antibodies at 4°C overnight and relevant secondary antibodies at room temperature for 1 h, the reaction was detected with enhanced chemiluminescence Western blotting detection reagents (Amersham Biosciences; ref. 22). Blot

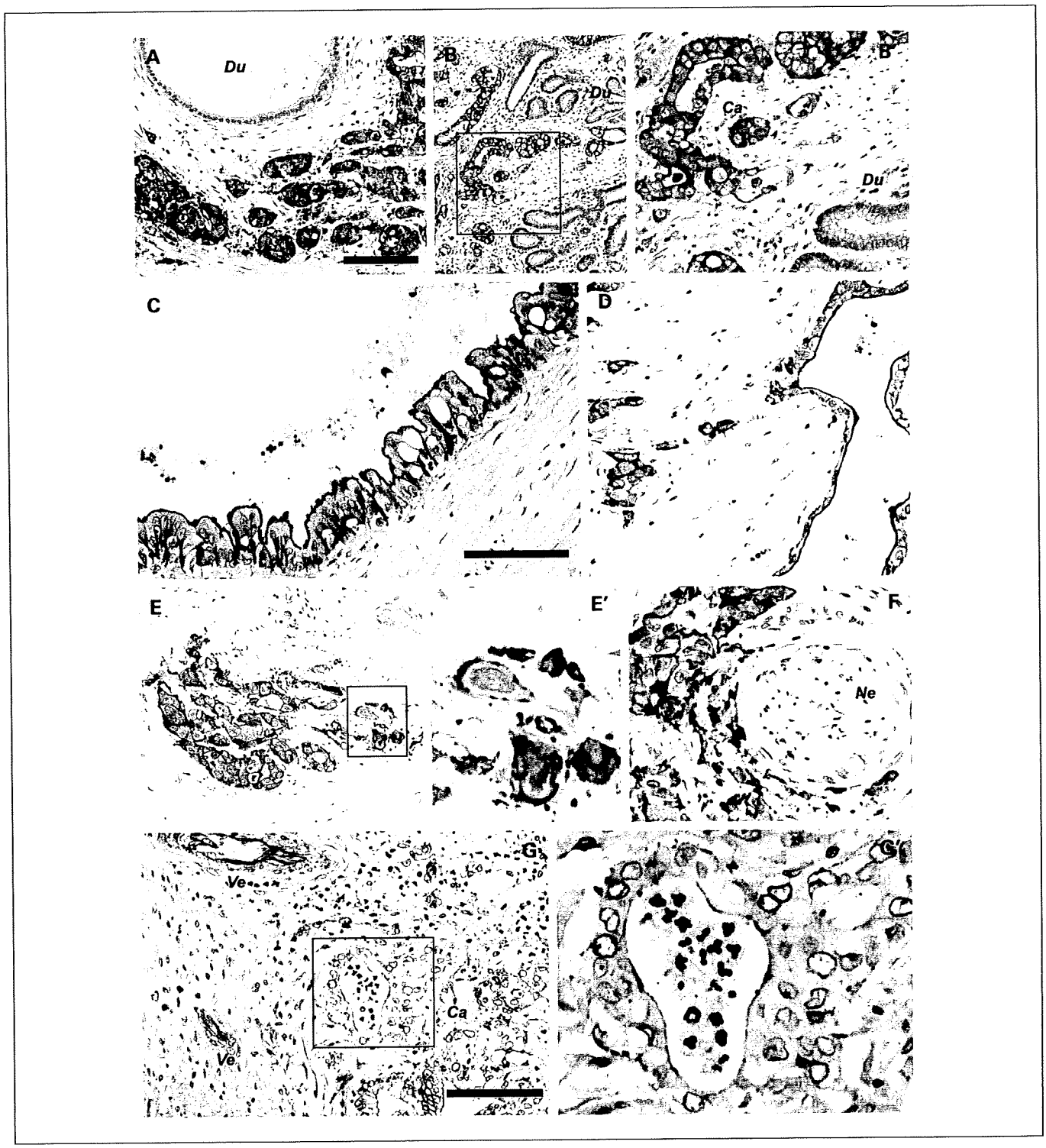

Fig. 1. Expression of actinin-4 in pancreatic cancer. Immunoperoxidase staining of actinin-4 in clinical samples of pancreatic cancer. *B'*, *E'*, and *G'*, insets from *B*, *E*, and *G*, respectively. Du, nonneoplastic pancreatic duct; Ca, cancer; Ne, peripheral nerve; Ve, blood vessels. Bars, 100 μm (*A* and *G*). Bar, 50 μm (*C*).

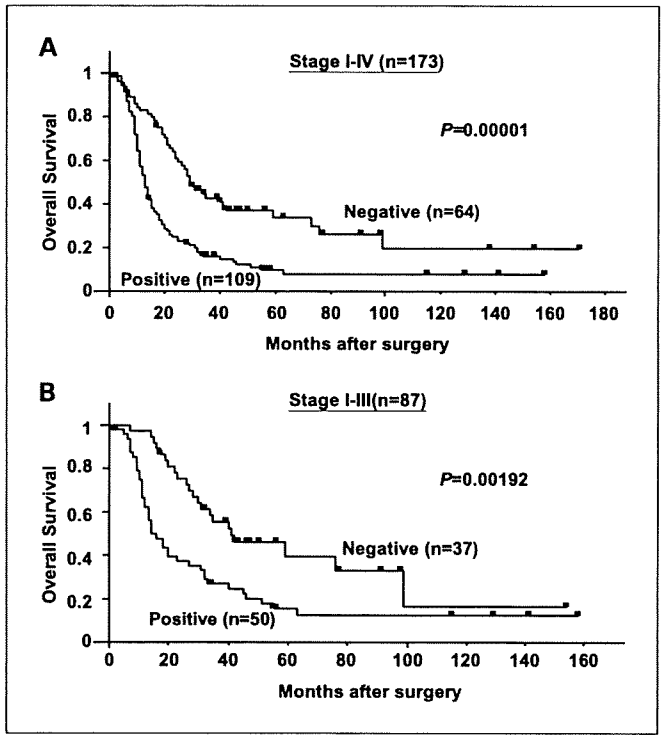

Fig. 2. Survival curves of patients positive and negative for actinin-4 expression. *A*, Kaplan-Meier analysis of overall survival for patients with clinical stage I to IV pancreatic ductal carcinoma (n = 173). Actinin-4 expression – positive cases (n = 109) had significantly poorer prognosis than expression-negative cases (n = 64; P = 0.00001, log-rank test). *B*, Kaplan-Meier analysis of overall survival for patients with clinical stage I to III pancreatic ductal carcinoma (n = 87). Actinin-4 expression – positive cases (n = 50) had significantly poorer prognosis than expression-negative cases (n = 37; P = 0.00192, log-rank test).

intensity was quantified with a LAS-3000 image analyzer and Multi-Gauze software (Fuji Film; ref. 23).

Fluorescence in situ hybridization analysis. Fluorescence *in situ* hybridization was done using the methods for PathVysion DNA probe kit (Abbott Molecular) as described previously (24). A representative formalin-fixed paraffin-embedded tissue block was selected by a pathologist (N. Hiraoka) and cut into 5-μm-thick sections. Hybridization was done at 37°C for 14 to 18 h with the denatured *ACTN4* (RP11-118P21) or *AKT2* (CTB-166E20) locus-containing bacterial artificial chromosome probe labeled with SpectrimOrange (Abbott Molecular). The specimen was counterstained with 4,6-dianidino-2-phenylindone. The number of fluorescence signals in 20 interphase tumor cell nuclei were counted independently by at least two investigators (S. Kikuchi and H. Tsuda or K. Onozato) and averaged.

Establishment of actinin-4 knockdown clones. *ACTN4* knockdown clones were established by the stable transfection of short hairpin RNA into BxPC-3 cells. A synthesized double-stranded oligonucleotide (5′-ggatggtcttgccttcaat-3′) targeting *ACTN4* mRNA was cloned into the pBAsi-hU6 Neo plasmid (Takara Bio), and the cells were transfected with LipofectAMINE 2000 reagent (Invitrogen). Twenty-four hours later, the transfection medium was replaced with RPMI 1640 containing 0.4 mg/mL of G418 (Geneticin, Invitrogen) to select clones with neomycin resistance.

Fluorescence cytochemistry. Cells grown on collagen-coated cover glasses (Asahi Technoglass) were fixed with 4% paraformaldehyde for 30 min at room temperature. The cells were incubated with anti-E-cadherin mouse monoclonal antibody and then with anti-mouse IgG Alexa Fluor 488 (Invitrogen). Filamentous actin fibers were visualized with Alexa Fluor 488 phalloidin (Invitrogen; ref. 25).

Scanning electron microscopy, cell migration assay, and cell growth assay. These assays and procedures are available online in the "Supplementary Methods."

Animal experiments. Female severe combined immunodeficiency mice (C.B-17/IcrCrl-scid) were purchased from Clea Japan and maintained in a specific pathogen-free environment. A laparotomy was done under general anesthesia, and 1×10^6 cells were injected orthotopically into the parenchyma of the pancreas with fine tuberculin needles, as described previously (26). The mice were sacrificed 5 weeks later, and serial sections of the entire pancreas were stained using H&E. The maximum diameter of the tumors was measured under a dissecting microscope (Nikon Instruments). All animal experimental procedures were reviewed and approved by the ethics committee of the National Cancer Center Research Institute (Tokyo, Japan).

Statistical analyses. Statistical analyses, including Kaplan-Meier analysis with log-rank test, χ^2 test, and the Cox proportional hazards regression model, were done with the StatFlex statistics package (version 5.0; Artiteck). The Wilcoxon rank sum test was done using a tool in the *R* project software package.[8]

Results

Expression of actinin-4 in invasive ductal carcinoma of the pancreas. The expression of actinin-4 protein was examined immunohistochemically in surgical specimens from 173 patients with pancreatic cancer (Fig. 1). The actinin-4 expression level in pancreatic cancer cells was increased compared with nonneoplastic duct epithelial cells (Fig. 1A and B). The expression of actinin-4 was limited to the apical and lateral membranes of cancer cells showing intraepithelial spreading (Fig. 1C), but this polarized distribution seemed to be lost in cancer cells that were dissociated from the glandular structure (Fig. 1D). Intense actinin-4 staining was observed in the periphery of cancer nests and in the membrane of solitary cells infiltrating the stroma (Fig. 1E and F).

Western blot analysis detected the expression of actinin-4 protein in 9 out of 11 (81.8%) pancreatic cancer cell lines examined, whereas AKT2 protein was detected only in Panc-1 cells (Supplementary Fig. S1).

Clinical significance of actinin-4 expression in pancreatic cancer. The staining intensity of actinin-4 was classified as "positive" when the actinin-4 expression level was equal to or higher than that of vascular endothelial cells, and "negative" when it was less than that of vascular endothelial cells (Fig. 1G). Of the 173 cases, there were 109 (63.0%) actinin-4 expression-positive cases and 64 (37.0%) expression-negative cases. The overall survival of positive cases was significantly worse than that of negative cases (P = 0.00001, log-rank test; Fig. 2A). Even in the 87 patients with clinical stages I to III, actinin-4 expression-positive cases had significantly poorer outcome than did expression-negative cases (P = 0.00192; Fig. 2B). Thirty-one (28.4%) out of the 109 actinin-4 expression-positive cases and 24 (37.5%) of the 64 actinin-4 expression-negative cases received postoperative chemotherapy (gemcitabine and others). There was no statistically significant difference in this respect between the groups (P = 0.2167, χ^2 test).

Univariate analysis with the Cox proportional hazards model (Table 1) revealed that clinical stage (P = 0.0062), extent of

[8] http://www.r-project.org

primary tumor (P = 0.0085), lymph node metastasis (P = 0.000001), distant metastasis (P = 0.000002), lymphatic invasion (P = 0.000076), and immunoreactivity of actinin-4 (P = 0.000012) were significantly correlated with the prognosis of the 173 patients with pancreatic cancer. Multivariate analysis indicated that actinin-4 expression was the most significant independent predictor of unfavorable prognosis (P = 0.000009; hazard ratio, 2.33; 95% confidence interval, 1.61-3.39),

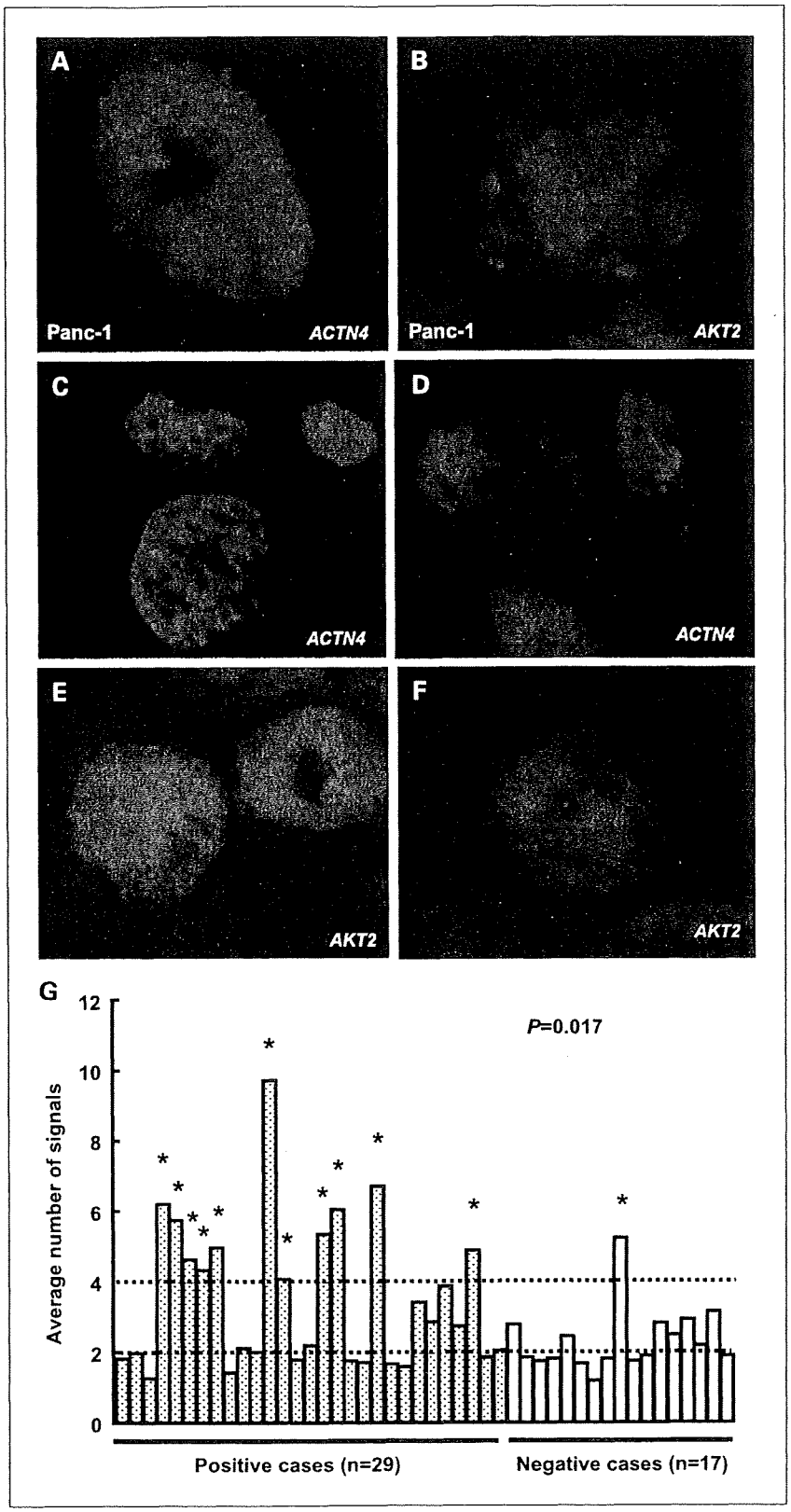

Fig. 3. Amplification of the *ACTN4* and *AKT2* genes in pancreatic cancer. *A-F*, fluorescence *in situ* hybridization analysis of copy numbers of the *ACTN4* (*A*, *C*, and *D*) and *AKT2* (*B*, *E*, and *F*) genes in a pancreatic cancer cell line (*Panc-1*; *A* and *B*) and clinical samples of pancreatic cancer (*C-F*). Increased copy numbers of the *ACTN4* (*C*) and *AKT2* (*E*) genes; two copies of the *ACTN4* (*D*) and *AKT2* (*F*) genes. *G*, correlation of actinin-4 protein expression and gene amplification. Average copy number of the *ACTN4* gene determined by fluorescence *in situ* hybridization in actinin-4 expression – positive cases (*gray columns*, n = 29) and expression-negative cases (*unshaded columns*, n = 17). Average signal number of <4 (per interphase nucleus) was defined as gene amplification (*). There is a significantly higher frequency of *ACTN4* amplification in actinin-4 expression – positive cases than in expression-negative cases (P = 0.017, χ^2 test).

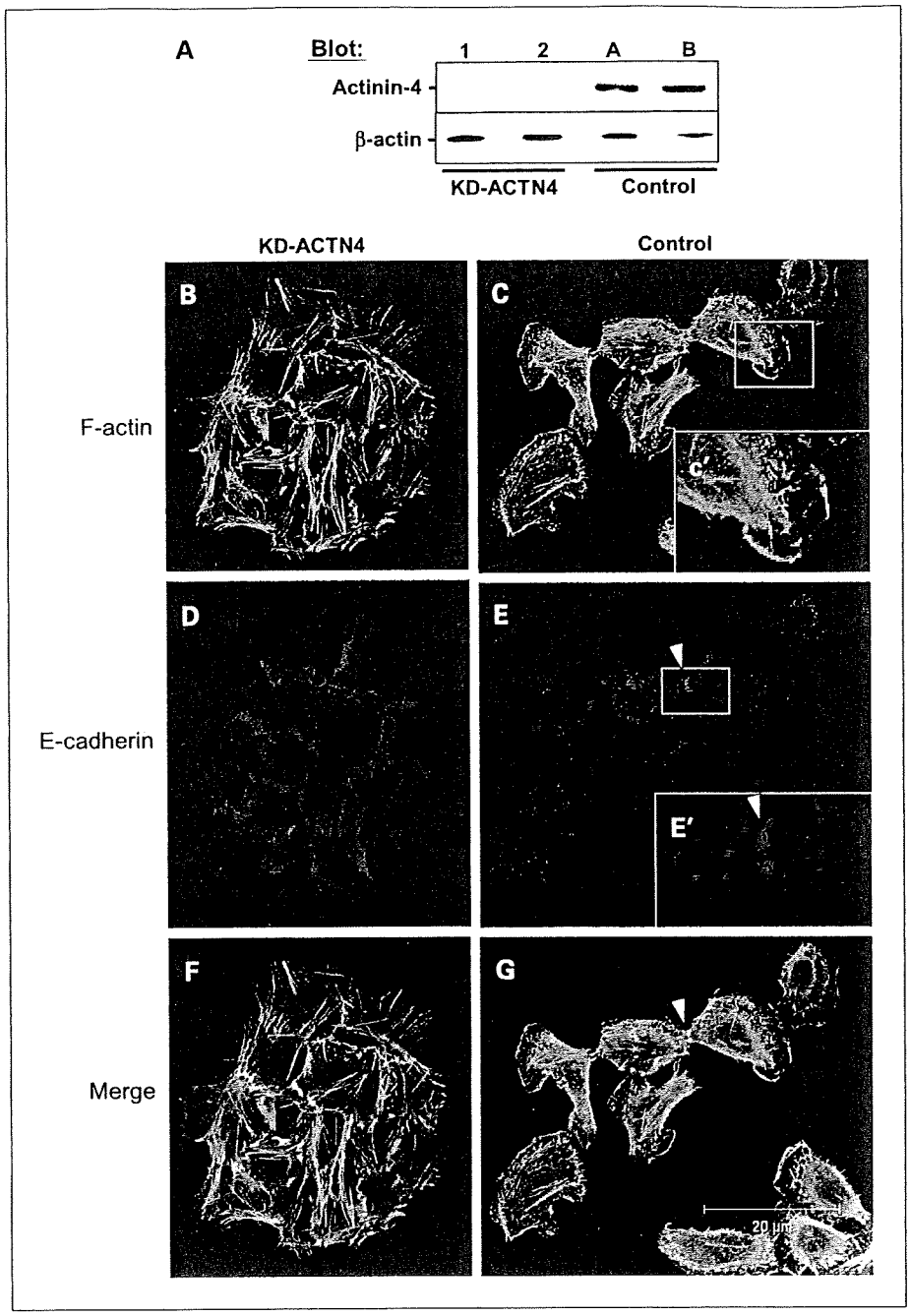

Fig. 4. Knockdown of actinin-4 alters cell morphology. *A*, Western blot analysis of actinin-4 and β-actin (loading control) protein expression in two stable clones in which expression of actinin-4 was knocked down by short hairpin RNA transfection (*KD-ACTN4, 1* and *2*) and two control clones (*Control, A* and *B*). *B-G*, immunofluorescence microscopic analysis of the actin cytoskeleton (*B, C*, and *green* in *F* and *G*) and E-cadherin expression (*D, E*, and *red* in *F* and *G*) in *ACTN4* knockdown (*KD-ACTN4*; *B, D*, and *F*) and control (*Control*; *C, E*, and *G*) cells. Filamentous actin (*F-actin*) was visualized by Alexa Fluor 488 phalloidin staining. *C'* and *E'*, insets from *C* and *E*, respectively. Arrowheads, intercellular connection (*E* and *G*).

followed by the presence of lymph node metastasis (P = 0.0073; hazard ratio, 1.96; 95% confidence interval, 1.20-3.19) and distant organ metastasis (P = 0.0050; hazard ratio, 1.73; 95% confidence interval, 1.18-2.54).

Gene amplification of ACTN4 in pancreatic cancer. Recurrent amplification of the chromosome 19q13 locus containing the *AKT2* gene has been reported in the pancreatic cancer cell line Panc-1. We investigated whether the *ACTN4* gene was included within the amplicon. Fluorescence *in situ* hybridization revealed an average of 13.7 *ACTN4* (Fig. 3A) and 27.0 *AKT2* (Fig. 3B) fluorescence signals per interphase Panc-1 cell. Consistently, real-time PCR showed that the copy numbers of the *ACTN4* and *AKT2* genes were increased 6-fold and 20-fold, respectively, in comparison with the immortalized near-diploid pancreatic ductal cell line H6C7 (Supplementary Fig. S2).

Fluorescence *in situ* hybridization was then done in surgical specimens of 46 randomly selected pancreatic cancers with positive expression of actinin-4 (n = 29) and negative expression of actinin-4 (n = 17; Fig. 3C-F). There was a significant difference in the frequency of *ACTN4* gene amplification between actinin-4 expression–positive and expression-negative cases (P = 0.017, χ^2 test), when gene amplification was defined as average fluorescence signals of >4 in 20 interphase tumor cell nuclei: 11 of 29 actinin-4 expression–positive cases (37.9%; gray columns; Fig. 3G) but only 1 of 17 expression-negative cases (5.9%; unshaded columns; Fig. 3G) showed gene amplification of *ACTN4*.

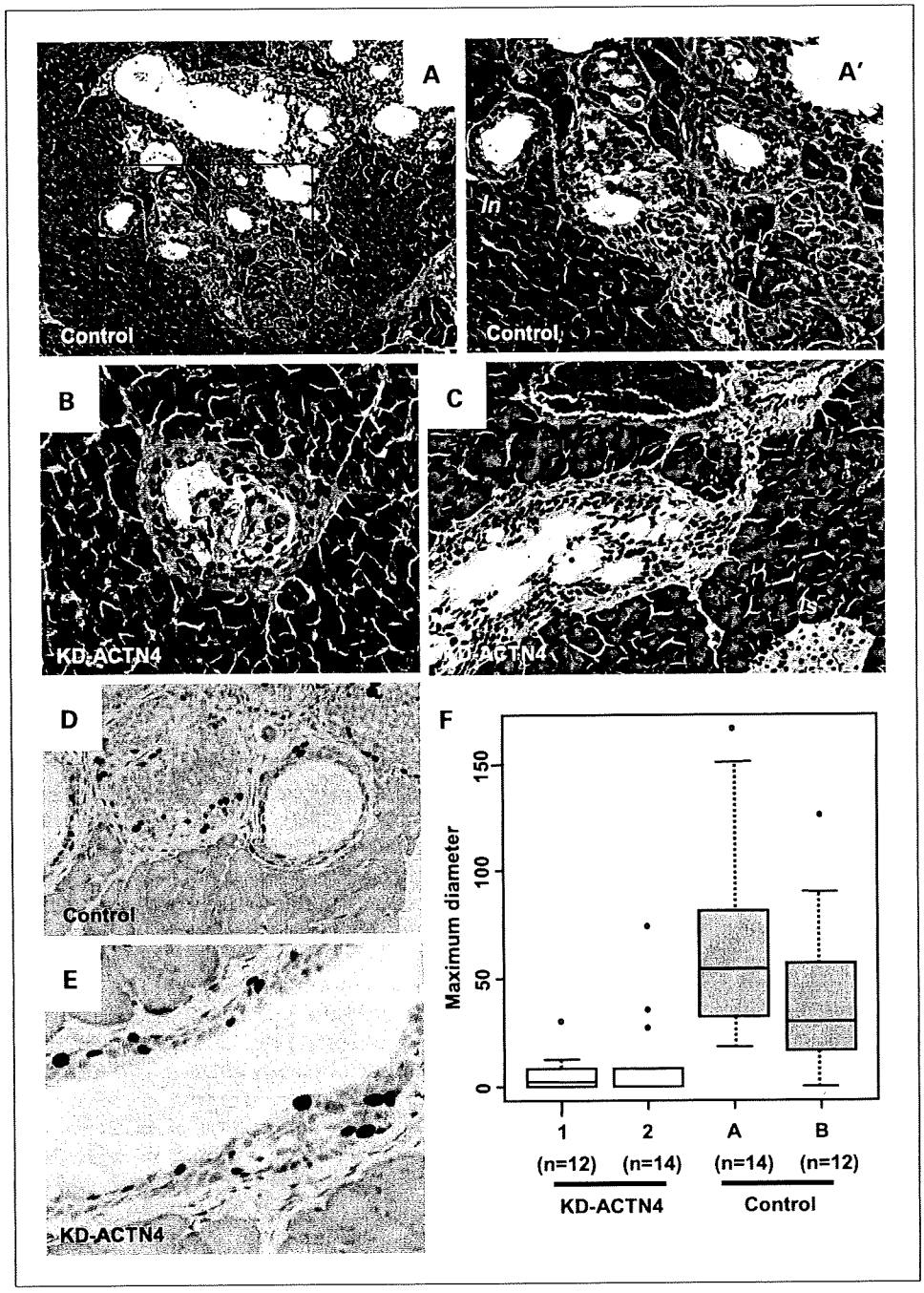

Fig. 5. Suppression of invasive growth by knockdown of actinin-4. *A-E*, H&E (*A-C*) and immunoperoxidase staining with anti-Ki67 antibody (*D* and *E*) of tumors generated by orthotopic implantation of *ACTN4* knockdown (*KD-ACTN4*; *B*, *C*, and *E*) and control (*Control*; *A* and *D*) cells into the pancreas of severe combined immunodeficiency mice. *A'*, inset in *A*. In, intraductal spreading; Du, normal pancreatic duct; Is, islet. *F*, whisker box-plot of maximum diameters (in 10^{-1} mm) of tumors generated by orthotopic implantation of *ACTN4* knockdown (*KD-ACTN4*, *1* and *2*) and control (*Control*, *A* and *B*) clones into the pancreas of severe combined immunodeficiency mice. There were significant differences between *ACTN4* knockdown and control clones ($P < 0.0001$ between KD-ACTN4-1 and Control A, $P = 0.0001$ between KD-ACTN4-2 and Control A, $P = 0.0024$ between KD-ACTN4-1 and Control B, and $P = 0.0071$ between KD-ACTN4-2 and Control B; Wilcoxon rank sum test).

Knockdown of ACTN4 expression. In order to examine the involvement of actinin-4 in the invasive growth of pancreatic cancer cells *in vivo*, we established, from the pancreatic cancer cell line BxPC3, two stable clones whose expression of actinin-4 had been knocked down by short hairpin RNA transfection (KD-ACTN4, lanes 1 and 2) and two control (nonsilencing) clones (Control, lanes A and B). We have previously reported that transient knockdown of actinin-4 expression by small interfering RNA significantly reduces the motility of BxPC3 cells in an *in vitro* migration assay (27). Western blot analysis confirmed the down-regulation of actinin-4 protein expression in the two knockdown clones (lanes 1 and 2; Fig. 4A), but not in the control clones (lanes A and B).

Knockdown of actinin-4 expression resulted in the alteration of cell shape and distribution of the actin cytoskeleton (Fig. 4B-G). Control cells were poorly connected, and filamentous actin was concentrated at the cell periphery (lamellipodia; Fig. 4C). Conversely, KD-ACTN4 cells showed tight intercellular connections, and marked extension of actin stress fibers along cellular long axes was observed (Fig. 4B). Actinin-4 competes with E-cadherin for binding to β-catenin (27). Knockdown of *ACTN4* may have restored the cell adhesion function of E-cadherin (Fig. 4D).

Scanning electron microscopy revealed the development of numerous microvilli on the dorsal surface of control cells (Control, Supplementary Fig. S3), whereas microvilli were

poorly developed in KD-ACTN4 cells (KD-ACTN4, Supplementary Fig. S3). Knockdown of actinin-4 expression reduced cell migratory activity (Supplementary Fig. S4).

Suppression of invasive growth by knockdown of actinin-4. Supplementary Fig. S5 illustrates the growth kinetics of KD-ACTN4 and control cells. KD-ACTN4 cells showed modest reduction of cell proliferation *in vitro*. However, the growth of KD-ACTN4 cells transplanted orthotopically into the pancreas of severe combined immunodeficiency mice was markedly suppressed (Fig. 5). Control cells formed masses at the sites of injection, destroying the parenchyma of the pancreas (Control; Fig. 5A) and spreading along the pancreatic ducts (*In*; Fig. 5A'). In contrast, KD-ACTN4 cells formed small nests in the connective tissue surrounding the pancreas (data not shown) or spread along the pancreatic ducts (KD-ACTN4; Fig. 5B and C). There were significant differences between the diameters of tumors generated by KD-ACTN4 clones and by control clones (Fig. 5F). However, Ki67 labeling revealed no apparent difference in cell proliferation activity between tumors generated by KD-ACTN4 and by control cells (Fig. 5D and E), consistent with the *in vitro* cell growth kinetics (Supplementary Fig. S5).

Discussion

Although the molecular mechanisms causing cancer invasion and metastasis are highly complicated, the acquisition of enhanced motility by cancer cells is a prerequisite. During the process of cell movement, actinin-4 protein levels are increased and highly concentrated at the leading edge of motile cells (4). We recently showed that increased expression of actinin-4 significantly enhances cell motility and mediates invasive growth and lymph node metastasis by colorectal cancer (6). In this study, actinin-4 was found to be overexpressed in the majority of invasive ductal carcinomas of the pancreas (Fig. 1), and increased expression of actinin-4 protein was significantly correlated with poor prognosis of patients with pancreatic cancer (Fig. 2). Knockdown of actinin-4 expression enhanced intercellular connections (Fig. 4) and significantly reduced the motility of a highly motile pancreatic cancer cell line (Supplementary Fig. S4; ref. 27). These observations lead us to conclude that actinin-4 plays a biologically significant role in pancreatic carcinogenesis.

We showed that gene amplification may underlie the increased expression of actinin-4 protein. Gene amplification of *ACTN4* was significantly more frequent in cases with increased expression of actinin-4 (Fig. 3G). However, several cases with increased expression of actinin-4 had a normal copy number of the *ACTN4* gene, and other molecular mechanisms could not be excluded. An invasive growth pattern seems to be an intrinsic feature of pancreatic cancer, and it is reasonable to assume that *ACTN4* is the target of the 19q13 amplification. Nevertheless, because several other candidate genes have been isolated from the chromosome region (16, 28, 29), the *ACTN4* gene may not be the sole target.

Recently, a familial pancreatic cancer gene on 4q32-34 was identified as *PALLD*, which encodes the protein palladin (30), another component of the actin-containing microfilaments that control cell shape, adhesion, and movement. Palladin binds to actinin and functions as a scaffold of the actin cytoskeleton (30, 31). The missense mutation of *PALLD* in the affected family was mapped to the actinin-binding domain of palladin (31). Transfection of the mutant palladin cDNA impaired the organization of the actin cytoskeleton and increased cell motility. Palladin mRNA was overexpressed in precancerous ductal dysplasia and carcinoma of the pancreas. Thus, *PALLD* mutation and palladin overexpression may have something to do with the functions of actinin-4.

Thus far, two non-muscle actinin isoforms, actinin-1 and actinin-4, have been identified. Enhanced actin stress fiber formation in KD-ACTN cells (Fig. 4B) may reflect a shift of filamentous actin from actinin-4 to actinin-1. A germ line mutation in the *ACTN4* gene is responsible for familial focal segmental glomerulosclerosis (32). Mice deficient in the *Actn4* gene manifest severe glomerular dysfunction (33), and failure of foot process extension by glomerular podocytes is thought be the major cause of focal segmental glomerulosclerosis. Knockdown of *ACTN4* in pancreatic cancer cells inhibited the formation of microvilli (Supplementary Fig. S3), probably through the same mechanism. Actinin-4 seems to be essential for the invasive growth of pancreatic cancer and may represent a candidate drug target. However, because of the lack of redundancy with actinin-1 in glomerular function, renal side effects may be a concern for therapeutics targeting actinin-4.

Actinin-4 is a multifunctional protein whose functional role is determined by partner proteins that form complexes with it. As well as the cell adhesion and cytoskeleton proteins, actinin-4 (or an unspecified non-muscle actinin) has been reported to interact with molecules of various functions, including BERP (34), Na^+/H^+ exchanger 3 (35), DNaseY (36), ATK1 (37), plasminogen activator inhibitor type-1 (38), histone deacetylase 7 (39), androgen receptor (40), and HER2/Neu/ErbB2 (41). For example, actinin-4 physically interacts with AKT1, and knockdown of *ACTN4* has been reported to inhibit the phosphorylation and nuclear translocation of AKT1. The AKT signaling pathway is known to be involved in regulating a variety of biological processes such as cell survival, proliferation, and motility (42).

In summary, we have identified increased expression and gene amplification of actinin-4 in pancreatic ductal carcinoma and clarified its clinical and biological significance. We believe that the findings reported here provide novel insights into diagnostic and therapeutic approaches to this devastating disease.

Disclosure of Potential Conflicts of Interest

No potential conflicts of interest were disclosed.

References

1. Landis SH, Murray T, Bolden S, Wingo PA. Cancer statistics, 1999. CA Cancer J Clin 1999;49:8–31.
2. Nitecki SS, Sarr MG, Colby TV, van Heerden JA. Long-term survival after resection for ductal adenocarcinoma of the pancreas. Is it really improving? Ann Surg 1995;221:59–66.
3. Lowenfels AB, Maisonneuve P. Epidemiology and prevention of pancreatic cancer. Jpn J Clin Oncol 2004;34:238–44.

4. Honda K, Yamada T, Endo R, et al. Actinin-4, a novel actin-bundling protein associated with cell motility and cancer invasion. J Cell Biol 1998;140:1383–93.
5. Yamagata N, Shyr Y, Yanagisawa K, et al. A training-testing approach to the molecular classification of resected non-small cell lung cancer. Clin Cancer Res 2003;9:4695–704.
6. Honda K, Yamada T, Hayashida Y, et al. Actinin-4 increases cell motility and promotes lymph node metastasis of colorectal cancer. Gastroenterology 2005; 128:51–62.
7. Furukawa T, Sunamura M, Horii A. Molecular mechanisms of pancreatic carcinogenesis. Cancer Sci 2006; 97:1–7.
8. Almoguera C, Shibata D, Forrester K, Martin J, Arnheim N, Perucho M. Most human carcinomas of the exocrine pancreas contain mutant c-K-ras genes. Cell 1988;53:549–54.
9. Hingorani SR, Petricoin EF, Maitra A, et al. Preinvasive and invasive ductal pancreatic cancer and its early detection in the mouse. Cancer Cell 2003;4:437–50.
10. Olive KP, Tuveson DA. The use of targeted mouse models for preclinical testing of novel cancer therapeutics. Clin Cancer Res 2006;12:5277–87.
11. Miwa W, Yasuda J, Murakami Y, et al. Isolation of DNA sequences amplified at chromosome 19q13.1-q13.2 including the AKT2 locus in human pancreatic cancer. Biochem Biophys Res Commun 1996;225: 968–74.
12. Hoglund M, Gorunova L, Andren-Sandberg A, Dawiskiba S, Mitelman F, Johansson B. Cytogenetic and fluorescence *in situ* hybridization analyses of chromosome 19 aberrations in pancreatic carcinomas: frequent loss of 19p13.3 and gain of 19q13.1-13.2. Genes Chromosomes Cancer 1998;21:8–16.
13. Mahlamaki EH, Kauraniemi P, Monni O, Wolf M, Hautaniemi S, Kallioniemi A. High-resolution genomic and expression profiling reveals 105 putative amplification target genes in pancreatic cancer. Neoplasia 2004;6:432–9.
14. Cheng JQ, Ruggeri B, Klein WM, et al. Amplification of AKT2 in human pancreatic cells and inhibition of AKT2 expression and tumorigenicity by antisense RNA. Proc Natl Acad Sci U S A 1996;93:3636–41.
15. Ruggeri BA, Huang L, Wood M, Cheng JQ, Testa JR. Amplification and overexpression of the AKT2 oncogene in a subset of human pancreatic ductal adenocarcinomas. Mol Carcinog 1998;21:81–6.
16. Kuuselo R, Savinainen K, Azorsa DO, et al. Intersex-like (IXL) is a cell survival regulator in pancreatic cancer with 19q13 amplification. Cancer Res 2007;67: 1943–9.
17. Shinoda Y, Kozaki K, Imoto I, et al. Association of KLK5 overexpression with invasiveness of urinary bladder carcinoma cells. Cancer Sci 2007;98: 1078–86.
18. Sobin L, Witteknd C. TNM classification of malignant tumors. 6th ed. New York: Wiley-Liss; 2002.
19. Japan Pancreas Society. Classification of pancreatic carcinoma. 2nd English ed., Tokyo: Kanehara & Co.; 2003.
20. Seike M, Kondo T, Mori Y, et al. Proteomic analysis of intestinal epithelial cells expressing stabilized β-catenin. Cancer Res 2003;63:4641–7.
21. Shimoyama Y, Hirohashi S, Hirano S, et al. Cadherin cell-adhesion molecules in human epithelial tissues and carcinomas. Cancer Res 1989;49:2128–33.
22. Yamada T, Takaoka AS, Naishiro Y, et al. Transactivation of the multidrug resistance 1 gene by T-cell factor 4/β-catenin complex in early colorectal carcinogenesis. Cancer Res 2000;60:4761–6.
23. Sato S, Idogawa M, Honda K, et al. β-Catenin interacts with the FUS proto-oncogene product and regulates pre-mRNA splicing. Gastroenterology 2005;129:1225–36.
24. Tsuda H, Akiyama F, Terasaki H, et al. Detection of HER-2/neu (c-erb B-2) DNA amplification in primary breast carcinoma. Interobserver reproducibility and correlation with immunohistochemical HER-2 overexpression. Cancer 2001;92:2965–74.
25. Honda K, Yamada T, Seike M, et al. Alternative splice variant of actinin-4 in small cell lung cancer. Oncogene 2004;23:5257–62.
26. Loukopoulos P, Kanetaka K, Takamura M, Shibata T, Sakamoto M, Hirohashi S. Orthotopic transplantation models of pancreatic adenocarcinoma derived from cell lines and primary tumors and displaying varying metastatic activity. Pancreas 2004;29:193–203.
27. Hayashida Y, Honda K, Idogawa M, et al. E-cadherin regulates the association between β-catenin and actinin-4. Cancer Res 2005;65:8836–45.
28. Moniaux N, Nemos C, Schmied BM, et al. The human homologue of the RNA polymerase II-associated factor 1 (hPaf1), localized on the 19q13 amplicon, is associated with tumorigenesis. Oncogene 2006;25: 3247–57.
29. Huntsman DG, Chin SF, Muleris M, et al. MLL2, the second human homolog of the Drosophila trithorax gene, maps to 19q13.1 and is amplified in solid tumor cell lines. Oncogene 1999;18:7975–84.
30. Pogue-Geile KL, Chen R, Bronner MP, et al. Palladin mutation causes familial pancreatic cancer and suggests a new cancer mechanism. PLoS Med 2006;3: e516.
31. Ronty M, Taivainen A, Moza M, Otey CA, Carpen O. Molecular analysis of the interaction between palladin and α-actinin. FEBS Lett 2004;566:30–4.
32. Kaplan JM, Kim SH, North KN, et al. Mutations in ACTN4, encoding α-actinin-4, cause familial focal segmental glomerulosclerosis. Nat Genet 2000;24: 251–6.
33. Kos CH, Le TC, Sinha S, et al. Mice deficient in α-actinin-4 have severe glomerular disease. J Clin Invest 2003;111:1683–90.
34. El-Husseini AE, Kwasnicka D, Yamada T, Hirohashi S, Vincent SR. BERP, a novel ring finger protein, binds to α-actinin-4. Biochem Biophys Res Commun 2000; 267:906–11.
35. Kim JH, Lee-Kwon W, Park JB, Ryu SH, Yun CH, Donowitz M. Ca(2+)-dependent inhibition of Na+/H+ exchanger 3 (NHE3) requires an NHE3-3KARP-α-actinin-4 complex for oligomerization and endocytosis. J Biol Chem 2002;277:23714–24.
36. Liu QY, Lei JX, LeBlanc J, et al. Regulation of DNaseY activity by actinin-α4 during apoptosis. Cell Death Differ 2004;11:645–54.
37. Ding Z, Liang J, Lu Y, et al. A retrovirus-based protein complementation assay screen reveals functional AKT1-binding partners. Proc Natl Acad Sci U S A 2006;103:15014–9.
38. Magdolen U, Schroeck F, Creutzburg S, Schmitt M, Magdolen V. Non-muscle α-actinin-4 interacts with plasminogen activator inhibitor type-1 (PAI-1). Biol Chem 2004;385:801–8.
39. Chakraborty S, Reineke EL, Lam M, et al. α-Actinin 4 potentiates myocyte enhancer factor-2 transcription activity by antagonizing histone deacetylase 7. J Biol Chem 2006;281:35070–80.
40. Jasavala R, Martinez H, Thumar J, et al. Identification of putative androgen receptor interaction protein modules: cytoskeleton and endosomes modulate androgen receptor signaling in prostate cancer cells. Mol Cell Proteomics 2007;6:252–71.
41. Wang SE, Shin I, Wu FY, Friedman DB, Arteaga CL. HER2/Neu (ErbB2) signaling to Rac1-1 is temporally and spatially modulated by transforming growth factor β. Cancer Res 2006;66:9591–600.
42. Testa JR, Bellacosa A. AKT plays a central role in tumorigenesis. Proc Natl Acad Sci U S A 2001;98: 10983–5.

Int. J. Cancer: **122,** 2707–2718 (2008)

Periostin, secreted from stromal cells, has biphasic effect on cell migration and correlates with the epithelial to mesenchymal transition of human pancreatic cancer cells

Atsushi Kanno[1], Kennichi Satoh[1]*, Atsushi Masamune[1], Morihisa Hirota[1], Kenji Kimura[1], Jun Umino[1], Shin Hamada[1], Akihiko Satoh[1], Shinichi Egawa[2], Fuyuhiko Motoi[2], Michiaki Unno[2] and Tooru Shimosegawa[1]

[1]*Division of Gastroenterology, Tohoku University Graduate School of Medicine, Sendai city, Miyagi, Japan*
[2]*Division of Hepatobiliary-Pancreatic Surgery, Tohoku University Graduate School of Medicine, Sendai city, Miyagi, Japan*

Periostin is a secretory protein that has been suggested to function as a cell adhesion molecule and promote the invasiveness or growth rate of tumors. However, little is known about the association of its expression and epithelial to mesenchymal transition (EMT), which is considered to play a crucial role in cancer cell metastasis. Thus, the authors investigated whether periostin could be involved in the process of EMT and the role of this gene in pancreatic cancer development. The expression of periostin was observed mainly in stromal cells but very little in cancer cells by immunohistochemistry and real-time RT-PCR. *In vitro*, pancreatic stellate cells (PSCs) exhibited a much higher basal expression of periostin compared with cancer cells. Periostin secreted in the supernatant from 293T cells that expressed periostin (approximately 150 ng/ml) inhibited the migration of pancreatic cancer cells. Coculture assay revealed that periostin expression in PSC was induced by pancreatic cancer cells. To assess the direct role of periostin in pancreatic cancer cells, the authors generated pancreatic cancer cell lines that stably express periostin. The induced expression of periostin (to 150 ng/ml) altered the morphology of cancer cells, changing them from mesenchymal to epithelial phenotypes with the induction of epithelial markers and a reduction of mesenchymal markers, and showed reduced cell migration *in vitro* and formed smaller tumors as well as suppressed metastasis *in vivo*. On the other hand, high concentration of recombinant periostin (1 μg/ml) promoted cell migration with AKT activation. The findings suggest that periostin has biphasic effect on the development of pancreatic cancer.
© *2008 Wiley-Liss, Inc.*

Key words: pancreatic cancer; periostin; EMT; pancreatic stellate cell

Pancreatic adenocarcinoma is one of the most malignant gastrointestinal tumors. Once pancreatic cancer is clinically evident, it progresses rapidly to develop metastatic lesions, frequently by the time of diagnosis. The pathogenic mechanisms that regulate the aggressive behavior of this cancer still remain to be clarified.

Tumor metastasis is a multistep pathological process involved in the final phase of tumor development. During this process, epithelium-derived tumor cells undergo fibroblast-like transformation, referred to as epithelial-mesenchymal transition (EMT).[1,2] EMT is the process by which an epithelial cell shows transitory changes in cell structure and becomes a more motile mesenchymal cell with migratory properties during embryogenesis. This transition is considered to be an important event during malignant tumor progression and metastasis.[3–5]

Periostin is a secretory protein that has been suggested to function as a cell adhesion molecule for preosteoblasts and to participate in osteoblast recruitment, attachment and spreading.[6,7] Recently, the expression of periostin has been implicated in the development of variety of carcinomas such as neuroblastoma,[8] epithelial ovarian cancer[9] and non-small cell lung carcinoma.[10] Periostin has been also reported to promote the metastatic growth of colon cancer by augmenting cell survival via the Akt/PKB pathway.[11] In addition, periostin has been suggested to promote the invasiveness or growth rate and confer resistance to hypoxia in pancreatic cancer cells, although the source of this protein was stromal cells rather than cancer cells.[12] It has been suggested that an interaction between cancer cells and stromal cells plays a pivotal role in cancer development since a pancreatic cancer cell supernatant stimulated the secretion of periostin from pancreatic satellite cells (PSC).[13] These findings raise the question of whether or not periostin can lead pancreatic cancer cells to the state of EMT through epithelial-mesenchymal interaction.

Here, we investigated the functional role of periostin during tumor progression *in vitro* and in *vivo*. We demonstrated that stromal cells were important sources of periostin and that pancreatic cancer cells increased the expression of periostin in PSC, which suppressed tumor metastasis through the blockade of EMT.

Material and methods

Tissues

Pancreatic cancer tissues were obtained from patients who underwent surgical operations for the tumors. The tissues collected at the time of surgery were fixed in 10% paraformaldehyde overnight and embedded in paraffin wax. Thirty-two pancreatic cancer tissues were used for the immunohistochemistry. Informed consent was obtained from all patients before surgery.

Immunohistochemistry

The localization of periostin in human pancreatic tissues was investigated by immunohistochemistry. The tissue sections were deparaffinized and the antigens were retrieved by boiling the sections in Target Retrival Solution (Dako, Carpenteria, CA) in a microwave oven. Then, the sections were incubated in methanol with 0.3% hydrogen peroxide for 30 min to block the endogenous peroxidase activity. After incubation with the periostin antibody (US Biological, Massachusetts, MA) overnight at 4°C, a histofine kit (Nichirei, Tokyo, Japan) was used. Visualization of the immunoreaction was carried out in 0.06 mM 3,3′-diaminobenzidine tetrahydrochloride (Dojin, Kumamoto, Japan) containing 2 mM hydrogen peroxide in PBS for several minutes at room temperature. For the negative control, the immunostaining process was performed by replacing the primary antibody with PBS. The negative control sections showed no specific immunoreactivity.

The degree of immunostaining was evaluated as follows: negative, no positive cells were found; weak, small clusters of positive cells were observed; moderate, clusters of positive cells were

Abbreviations: 293T-peri, periostin expressing vector transfected cells; BrdU, 5-bromo-2-deoxyuridine; EMT, epithelial to mesenchymal transition; EV cells, empty vector transfected cells; GAPDH, glyceraldehyde-3-phosphate dehydrogenase; HUVEC Human umbilical vein endothelial cells; Panc1.EV, empty vector transfected Panc1 cells; PP1, Panc1 cells stably overexpressing periostin; PSC, pancreatic stellate cells; RT-PCR, reverse transcription-polymerase chain reaction.

Grant sponsor: Ministry of Education, Science, Sports and Culture in Japan; Grant numbers: 17390213 and 19590745.

***Correspondence to:** 1-1, Seiryo-machi, Aobaku, Sendai city, Miyagi, 980-8574, Japan. Fax: +[81-22-717-7177].
E-mail: ksatoh@mail.tains.tohoku.ac.jp

Received 8 June 2007; Accepted after revision 5 November 2007
DOI 10.1002/ijc.23332
Published online 1 April 2008 in Wiley InterScience (www.interscience.wiley.com).

observed in some areas; and intense, immunoreactive cells were observed in most areas of tissue sections. The evaluation of immunostaining was done independently by 2 observers (K.S. and A.K.) who had not been informed of the histological diagnosis.

RNA extraction and RT-PCR for pancreatic cancer cell lines and tissues

Total RNA was prepared using the RNeasy kit (QIAGEN, Hilden, Germany) with DNase I treatment to eliminate any DNA contamination according to the protocol provided by the manufacturer. First strand cDNA was generated from 1 μg total RNA using RETROscript kit (Ambion, Austin, TX) according to the manufacturer's protocol. PCR was performed on 2 μl of RT products in a 25-μl reaction mixture using Ex Taq polymerase (Takara, Ohtsu, Japan) with 10 μmol/l of 3′ and 5′ primers. The gene expression was normalized to the respective glyceraldehydes-3-phosphate dehydrogenase (GAPDH) expression level. The PCR condition for our cDNA templates was set to ensure that replication was in the linear phase for each primer set used. To quantify the gene expression level, we also employed quantitative real-time RT-PCR by using LightCycler and LightCycler-FastStart DNA Master SYBR Green I (Roche diagnostics, Basel, Switzerland). Each experiment was repeated at least 3 times, and representative data are shown. The primer pairs used were as follows: human periostin, forward 5′ TGTTGCCCTGGTTATATGAG3′ and reverse 5′ACTCGGTG CAAAGTAAGTGA3′; rat periostin, forward 5′TGCAAAAAGA GGTCTCCAAGGT3′ and reverse 5′AGGTGTGTCTCCCTGAA GCAGT3′; human GAPDH, forward 5′GGCGTCTTCACCACCA TGGAG3′ and reverse 5′AAGTTGTCATGGATGACCTTGGC3′; rat GAPDH, forward 5′ACATCATCCCTGCATCCACT3′ and reverse 5′GGGAGTTGCTGTTGAAGTCA3′. The annealing temperature for these primer sets was 58°C. All reactions were performed according to the manufacturer's protocol. The specificity of each PCR reaction was confirmed by melting curve analyses. The primers for rat periostin and GAPDH did not detect human periostin or GAPDH (data not shown). The level of target gene expression in each sample was normalized to the respective GAPDH expression level.

Pancreatic tissue samples and microdissection

The pancreatic tissues collected at the time of surgery were embedded immediately in Tissue-Tek OCT compound medium (Sakura, Tokyo, Japan), frozen in liquid nitrogen and stored at −80°C. The frozen tissues were cut into 8-μm-thick sections using a crsyostat (Jung CM3000; Leica, Nussloch, Germany) and then fixed with cold methanol and stained with toluidine blue. Histologically cancerous ductal cells and stromal cells from the sections were dissected using LaserScissors Pro300 (Cell Robotics, Albuquerque, NM) according to the manufacturer's protocols. These microdissected samples were subjected to RNA extraction. RNA was prepared using the RNeasy Micro kit (QIAGEN, Hilden, Germany) with DNase I treatment to eliminate DNA contamination according to the protocol provided by the manufacturer.

Cell culture and isolation

The human pancreatic cancer cell lines (AsPC-1, BxPC3, Panc-1 and MIAPaca2) were purchased from American Type Culture Collection (Manassas, VA), routinely grown in Dulbecco's Modified Eagle Media (DMEM) containing 10% fetal bovine serum (Miles, Kankakee, IL) at 37°C, 5% CO_2 in a humidified environment. Four colonic cancer cell lines (WiDr-Tc, SW480, CoLo205, DLD1), human fibroblast (KMST6) and human embryonic kidneyfibroblast cell line (293T), which were provided by Cancer Cell Repository (Institute of Development, Aging and Cancer, Tohoku University, Sendai, Japan), were cultured in Dulbecco's modified Eagle's medium (DMEM) containing 10% heat-inactivated fetal bovine serum, penicillin sodium and streptomycin sulfate. Human pancreatic stellate cells (PSCs) were isolated from the surgically resected normal pancreas tissues of patients with pancreatic cancer,[14] under the approval of the Ethics Committee of Tohoku University School of Medicine. The cells were maintained in Ham's F-12/DMEM containing 10% heat-inactivated fetal bovine serum (ICN Biomedicals, Aurora, OH), penicillin sodium and streptomycin sulfate. Human umbilical vein endothelial cells (HUVEC) and their optimized culture medium were purchased from Clonetics (San Diego, CA). HUVEC were grown on 0.2% gelatin-coated tissue culture dishes (Corning, Corning, NY). Immortalized rat PSC line (SIPS) isolation and culture were performed as previously described.[15]

Coculture of rat pancreatic stellate cell line (SIPS) and Panc1

Panc1 cells were added to monolayer of immortalized rat PSCs (1×10^6 cells/10 mm dish) at a ratio of 1:1 and cultured for 24 hr at 37°C. Total RNA was extracted, and the levels of rat periostin mRNA in the immortalized rat PSCs were investigated by real-time RT-PCR.

Generation of periostin-overexpressing Panc1, KMST6, 293T cells

The expression plasmid of HA-tagged rat periostin was kindly provided by Dr. Inoue (Siga University, Japan). Transfection of the cells with expression vectors (rat periostin cDNA or vector alone) was performed using FuGENE 6(Roche, Indianapolis, IN) as recommended by the supplier. Transfected Panc1 and KMST6 were selected with 800 mg/ml of G418 (Invitrogen) to generate stably expressing cell lines. After G418 selection, the clones were subjected to immunoprecipitation and Western blot analysis with a specific antibody against HA to confirm the periostin expression. After establishment of the empty vector (EV) or periostin transfected clonal cell lines, the same passages were used for each experiment.

Reagent

Recombinant human periostin was purchased from Biovendor (Heidelberg, Germany). Periostin treatment was performed in 0.1 M acetate buffer (pH4) at the concentration of 100 ng/ml or 1 μg/ml.

Immunoprecipitation

Immunoprecipitation was performed using a protein G immunoprecipitation kit (Roche Applied Science) according to the manufacturer's instructions. Briefly, 500 μg of protein from cell lysates or supernatant were incubated with 1 μg of anti-HA antibody at 4°C for 1 hr. Fifty microliters of protein G (provided with the kit) were used per sample. Western blot analysis was performed as described later.

Western blot analysis

For whole cell protein extraction, cells were lysed by the addition of lysis buffer (150 mM Tris-HCl, pH 7.4, 1% NP-40, 0.5% sodium deoxycholate). The protein concentration in each sample was determined using a Bradford assay kit (Dojin, Kumamoto, Japan). After the addition of 5 × sample buffer (pH 6.8, 125 mM Tris-HCL, pH 6.8, 4% sodium dodesylsulphate, 20% glycerol and 0.04% bromphenolblue, 10% mercaptoethanol), aliquots were boiled at 100°C for 5 min and subjected to Western blotting. The nitrocellulose membrane (Bio-Rad Laboratories, Hercules, CA) was blocked for 1 hr at room temperature in a buffer containing 10 mM Tris-HCL (pH 7.5), 100 mM NaCl, 0.1% Tween 20 and 5% dry milk, and then incubated with primary antibody overnight at 4°C. The primary antibodies used in this study were as follows: HA antibody (Sigma, St Louis, MO), monoclonal mouse E-cadherin antibody (BD Transduction Laboratories, Lexington, KY), monoclonal mouse β-catenin antibody (BD Transduction Laboratories), monoclonal mouse phosphospecific Akt antibody (BD Transduction Laboratories) and monoclonal mouse total Akt antibody (BD Transduction Laboratories). The membrane was washed with a buffer containing 10 mM Tris-HCl, pH 7.5, 100 mM NaCl,

0.1% Tween 20 and incubated with anti-rabbit or mouse-immunoglobulin G coupled to peroxidase (Amersham Bioscience, Buckinghamshire, UK) for 1 hr at room temperature. Reactive bands were detected using ECL chemiluminesence reagent (Amersham Bioscience). The specific bands were subjected to densitometry analysis by using the ImageJ program provided by the National Institutes of Health (Bethesda, MD).

Enzyme-linked immunosorbent assay

After 24-hr incubation, periostin levels in the culture supernatant were determined by the enzyme-linked immunosorbent assay (ELISA). Briefly, ELISA immunoassay plates (Becton Dickson, Franklin Lakes, NJ) were coated with the samples overnight at 4°C. After coating, the plates were incubated with 5% dry milk to block uncoated sites. After washes with phosphate-buffered saline, rabbit anti-periostin antibody (at 1:2000 dilution) was added and incubated for 1 hr at room temperature. After washes, goat anti-rabbit IgG antibody conjugated with horseradish peroxidase (Southern Biotechnology, Birmingham, AL) was added and incubated for 1 hr. After final washes, 3,3′,5,5′-tetramentylbenzidine (Pierce, Rockford, IL) was added. The periostin concentration was determined by differences in absorbance at wavelength 450 minus 550 nm. Recombinant periostin served as a standard control.

Fluorescent immunohistochemistry

Periostin- or EV-transfected Panc1 cells were grown to subconfluence on BD Falcon™ culture slides (BD Biosciences, San Jose, CA) and fixed with cold methanol (Wako, Osaka, Japan). After blocking with normal goat serum, the cells were incubated with mouse monoclonal E-cadherin antibody (BD Transduction Laboratories) and monoclonal mouse β-catenin antibody(BD Transduction Laboratories) overnight at 4°C and then the slides were incubated with fluorescein-conjugated goat anti-mouse IgG (Jackson ImmunoReserch laboratories, West Grove, CA). Cells were then incubated with propidium iodide (Wako) for nuclear staining and mounted with Vectashield (Vector Laboratory). For double staining for periostin and α-SMA, cells were fixed with cold methanol. After blocking with 3% bovine serum albumin in PBS, the cells were incubated with rabbit polyclonal anti-periostin antibody and mouse polyclonal α-SMA antibody overnight at 4°C and then the slides were incubated with Alexa Fluor 546 donkey anti-goat IgG (Molecular Probes) and Alexa Fluor 488 donkey anti-rabbit IgG (Molecular Probes, Eugene), respectively, and mounted with Vectashield (Vector Laboratory). Cells were visualized for immunofluorescence with a Confocal TIRF-C1 microscope (Nikon Intstech, Kawasaki, Japan).

Cell growth assays

Cell growth was assessed by direct count and 5-bromo-2-deoxyuridine (BrdU) assay. For the direct count, pancreatic cancer cells were grown in 6-well culture dishes (BD Falcon) with normal growth media. Cells were counted using a hemocytometer every day (days 1, 2, 3, 4 and 5) after removing the cells from the plates with 0.5 g/l trypsin. For BrdU assay, 6,000 periostin-transfected cells or EV cells were seeded per well in 96-well plates (BD Falcon) in normal cell growth media. The BrdU assay was performed after 24, 48 and 72 hr incubation using a kit (Roche) according to the manufacturer's protocol. For each cell line, the proliferation index was evaluated and absorbance at 48 and 72 hr was normalized to that at 24 hr.

Scrape motility assay

Pancreatic cancer cells were grown to confluency in 12-well culture dishes (BD Falcon) with normal growth media. The cell monolayer was mechanically scratched with a sterile pipette tip. Subsequently, the plates were incubated with serum-free DMEM including recombinant periostin (0 to 1 μg/ml) or the supernatant from periostin-expressing or control 293T cells for additional 2 to 4 days. Cells were visualized with an Olympus MODEL CK2 inverted microscope using a 10× objective. Images were captured in a time-lapse manner with an Olympus C2000 digital camera. The scratched area covered by migrated cells was measured in 3 independent wells and normalized to the initially scratched area using Scion Image Software (Scion Corporation).

Two-chamber migration assays

Cell invasion was determined by using a modified 2-chamber migration assay (pore size of 8 mm, BD Biosciences) according to the manufacturer's instructions. 2.5×10^4 cells were seeded in serum-free medium in the upper chamber and migration during 24 hr toward the lower chamber which contained 10% FBS as a chemoattractant was evaluated. Cells in the upper chamber were carefully removed using a cotton bud, and cells at the bottom of the membrane were fixed and stained with Diff-Quick (International Reagents, Kobe, Japan). Quantification was performed by counting the stained cells.

Soft agar assay

Forty thousand PP1 or Panc1.EV cells per well were suspended in 0.3% Bacto ™ agar (BD Falcon) supplemented with DMEM medium containing 10% fetal bovine serum and were layered over 1 ml of a 0.8% agar-medium base layer in 6-well plates. After 21 days, viable colonies were stained with nitroblue tetrazolium (Roche) and anchorage-independent growth was estimated by counting the number of stained colonies using a high power microscope.

Tumor growth in nude mice

Tumor formation *in vivo* was assessed in female athymic nude mice by subcutaneous injection of 2×10^6 cells each, suspended in 200 μl of sterile PBS. The tumor volume was measured every week after the first detection of visible tumor formation. Volume was determined by the equation $V = L \times W^2 \times 0.5$, where V is volume, L is length and W is width. The mice were sacrificed 7 weeks after injection and the histology was examined by H&E staining.

Orthotopic implantation

To assess metastasis formation, periostin and EV-transfected Panc1 cells (1×10^6 cells suspended in 50 μl) were injected into the pancreatic tail of female athymic nude mice. The mice were sacrificed 9 weeks after injection and tumor progression was confirmed. Histology was evaluated by H&E staining.

Statistical analysis

Statistical analysis was performed and graphs were made with GraphPad Prism software (GraphPad Software, San Diego, USA). The correlation of periostin expression with the patients' clinicopathological variables and the correlation between periostin expression and frequency of metastasis in the orthotopically injected mice were analyzed by χ^2 test. The difference between 2 groups was analyzed by unpaired t test or Mann–Whitney U test. The p value <0.05 was regarded as statistically significant.

Results

Periostin expression and localization in pancreatic tissue and pancreatic cell lines

To evaluate the expression of periostin in the pancreatic tissues, immunostaining was performed in 61 human pancreatic tissues (2 normal pancreatic tissue, 32 pancreatic cancer, 13 intraductal papillary mucinous neoplasms and 10 chronic pancreatitis) and 4 cases of colonic cancer. The expression of periostin was not detected in pancreatic caricinoma cells, normal pancreatic ductal cells or colonic carcinoma cells. However, there was strong expression in the stromal cells adjacent to the epithelial cells in pancreatic and colonic tissues (Figs. 1*a*–1*d*, Table I). Since strong immunoreactivity was present in the stroma of pancreatic and

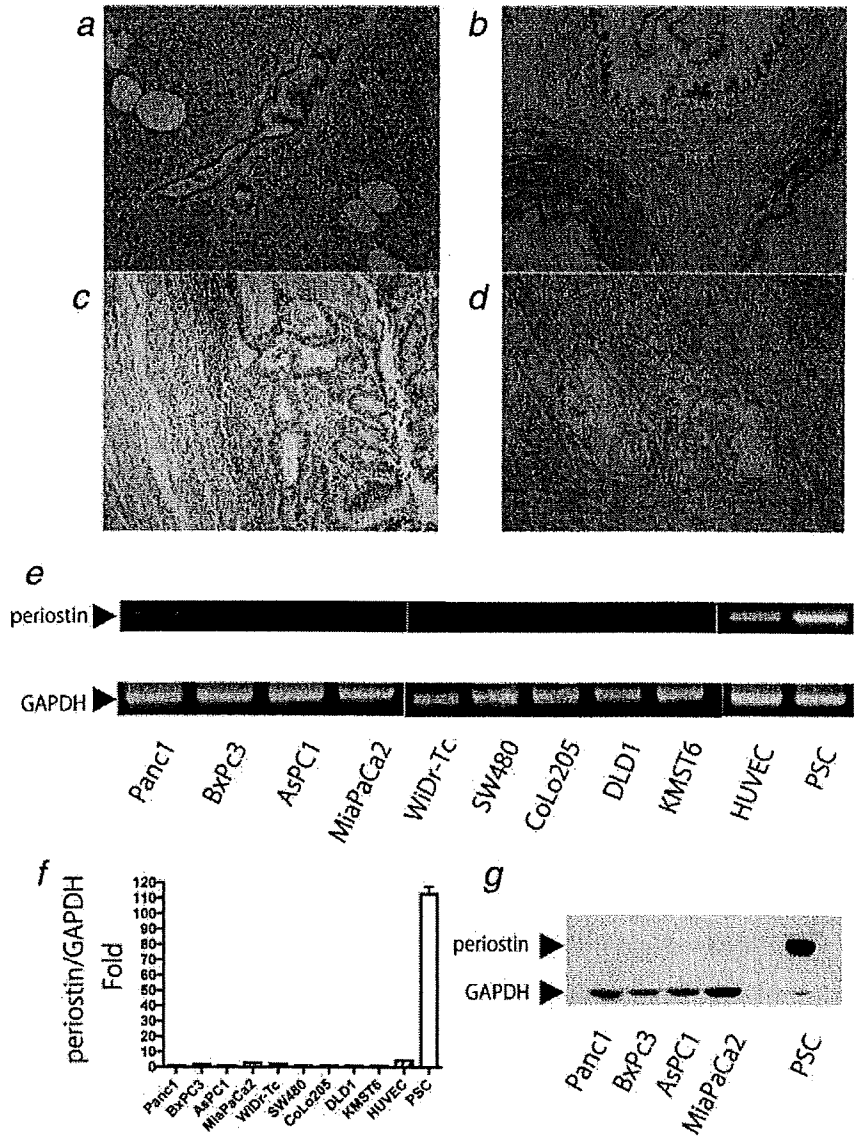

FIGURE 1 – Periostin expression in normal tissue of pancreas (*a*), IPMN (*b*), pancreatic cancer (*c*) and colonic cancer (*d*). *a*, Normal pancreatic duct and acinar cells showed no staining for periostin. *b–d*, Stromal areas of the sections showed positive staining for periostin, but tumor lesions showed no staining for periostin. *e–g*, Periostin expression in pancreatic cancer cell lines, colonic cancer cell lines and normal cultured cells (HUVEC, PSC). Periostin expression in cultured cells was examined by RT-PCR (*e*), quantitative real-time RT-PCR (*f*) and Western blot analysis (*g*). The expression of periostin mRNA was detected in PSC and in HUVEC while no or little expression was observed in carcinoma cell lines or KMST6 (fibroblastic cells). *f*, Expression of periostin mRNA was normalized to that of GAPDH mRNA. Values are expressed relative to 1.00 for expression in Panc-1 cells. Real-time RT-PCR clearly indicates the difference in the expression levels of periostin between pancreatic cancer cell lines and normal cultured cells. The highest expression was seen in PSC. *g*, Western blot analysis clearly showed that the expression of periostin protein is detected in PSC but not in pancreatic cancer cell lines.

TABLE I – THE ASSOCIATION OF THE EXPRESSION OF PERIOSTIN WITH EPITHELIAL DUCT OR STROMAL CELLS

	Cancer	Stroma	*p*-value
Pancreatic cancer (n = 32)	2/32	30/32	$p < 0.05$
IPMN (n = 13)	2/13	13/13	
Chronic pancreatitis (n = 10)	0/10	10/10	
Colonic cancer (n = 4)	0/4	4/4	

For the evaluation of the periostin expression, chi square test and fisher exact test were performed.

colonic carcinoma tissues, we investigated the expression of periostin by RT-PCR in cultured cell lines of various origin to elucidate the source of this gene. The cultured cell lines we used were primary cultures of human PSCs, cultured pancreatic cancer cells (Panc1, AsPC1, MiaPaCa2, BxPC3), cultured colonic cancer cells (WiDr-Tc, SW480, CoLo205, DLD1), cultured human fibroblasts (KMST6) and HUVEC. Among these cell lines, the expression of periostin mRNA was detected in HUVEC and PSC while little or no expression of this gene was found in pancreatic and colonic cancer cell lines (Fig. 1*e*). The quantitative real-time RT-PCR

showed a difference in the periostin expression level and revealed higher expression in normal cultured cells (PSC or HUVEC) than in carcinoma cells (Fig. 1*f*). Western blot analysis also revealed that the expression of periostin protein was detected only in PSC but not in pancreatic cancer cell lines (Fig. 1*g*).

Periostin expression was increased in peritumoral stroma

To determine the source of periostin in human pancreatic cancer tissues, double immunofluorescence immnohistochemistry was performed using periostin and α-SMA antibodies on frozen tissue sections. As shown in Figure 2*a*, stromal cells adjacent to carcinoma cells coexpressed periostin and α-SMA, suggesting that periostin was localized in mesenchymal cells. To compare the intensity of gene expression between the carcinoma lesion and stromal area, the ductal adenocarcinoma lesion and stromal area were carefully microdissected and were subjected to quantitative real-time RT-PCR (Fig. 2*b*). As shown in Figure 2*b* (b and c), stromal cells expressed significantly higher level of periostin than did cancer cells. These findings indicate that stromal cells but not carcinoma cells are a source of periostin in human pancreatic cancer tissues.

Periostin plays an important role in epithelial mesenchmal interaction

Because periostin is a secretory protein that was found abundantly in the stromal area as described earlier, we analyzed the effect of secreted periostin on pancreatic cancer cells. We established 293T cells transiently expressing periostin and collected the supernatant where periostin expression was clearly detected (Fig. 3*a*). Using this supernatant, we examined the cell migration ability of Panc1 cells by wound healing scratch assay. As shown in Figure 3*b*, Panc1 cells with the supernatant from 293T-peri cells did not cover the scratched area with migrating cells while those with the supernatant from control 293T cells showed many cells in the scratched area, indicating that secreted periostin inhibits the cell migration of pancreatic cancer cells. Taken together with the results that stromal cells but not cancer cells were the source of periostin, we hypothesized that secreted periostin from stromal cells inhibits the migration of pancreatic cancer cells. Therefore, we next investigated whether pancreatic cancer cells had an effect on stromal cells in cocultured system. Panc1 and rat PSC cells were cocultured in a contact condition, as described in Material and Methods, and the expression level of rat-periostin was determined after 24 hr of incubation by real-time RT-PCR analysis using specific primers for rat periostin that did not recognize human periostin (Fig. 3*c*). As shown in Figure 3*d*, the significant induction of periostin mRNA that originated from PSC was observed only when PSC was cocultured with Panc1, suggesting that pancreatic cancer cells could induce the expression of periostin in PSC.

To confirm the interaction between carcinoma cells and stromal cells *in vivo*, pancreatic cancer cells (BxPC3) were subcutaneously injected into nude mice with periostin overexpressing (KMSTp18) or control fibroblastic cell lines with EV (KMST6). In all animals, pancreatic carcinoma cells with control fibroblastic cells grew faster than those with periostin expressing fibroblastic cells. In addition, BxPC3 coinjected with KMST6 showed significantly larger tumors compared with BxPC3 coinjected with KMSTp18 (Fig. 3*e*). These findings suggested that secreted periostin from stromal cells inhibit pancreatic cancer cell growth *in vivo*.

Generation of stable periostin-expressing cell line

Since secreted periostin suppressed the migration or growth of pancreatic cancer cells *in vitro* and *in vivo*, we postulated that this gene functions as a tumor suppressor in pancreatic carcinoma cells. Therefore, we generated stably expressing pancreatic cancer cells. Panc1 cells were transfected with periostin expression vector and were cloned, and the expression of this gene was confirmed by quantitative real-time RT-PCR and Western blot. Among several clones expressing periostin mRNA, we confirmed one clone (PP1) which also expressed periostin protein (Figs. 4*a*–4*c*). A morphological difference was observed between control (parental and EV transfected Panc1) and priostin expressing Panc1 cells (PP1). Control cells fundamentally showed loose cell attachment and scattered morphology like mesenchymal cells, while PP1 demonstrated cobblestone-like appearance (Fig. 4*d*).

Expression of periostin-induced epithelial characteristics

To investigate whether the enhanced expression of periostin would affect epithelial and mesenchymal markers in cultured tumor cells *in vitro*, we performed immunofluorescence staining and western blot analysis for epithelial and mesenchymal markers on periostin- or EV-transfected Panc1 cells. As shown in Figure 3*e*, PP1 cells showed dominant membrane-bound staining of E-cadherin and β-catenin while control cells (Panc1.EV) exhibited a weak and diffuse distribution of epithelial markers. In contrast, the expression of mesenchymal markers (vimentin and N-cadherin) was reduced in PP1 cells compared with control cells (Panc1.EV). Consistent with these findings, western blot analysis also showed increased expression of epithelial markers (β-catenin, E-cadherin) and decreased expression of mesenchymal markers (N-cadherin, Vimentin). These molecular changes implied that the induced expression of periostin shifted the Panc1 cells from the mesenchymal to epithelial phenotype.

Expression of periostin results in interference with cell migration, and spread in vitro

To assess the effects of periostin on pancreatic cancer proliferation, cell count assay (Fig. 5*a*) and BrdU incorporation assay (Fig. 5) were performed. Neither of these analyses showed significant differences in cell proliferation between controls and periostin-expressing cells. To elucidate the function of periostin in the anchorage-independent growth of pancreatic cancer cells, we utilized the soft agar assay. PP1 and control cells showed similar numbers of colonies on soft agar (Fig. 5*c*).

We next examined the cell migration ability of PP1 cells by wound healing scratch assay. As shown in Figure 5*d*, Panc1.EV cells covered the scratched area with migrating cells within 48 hr but periostin expressing cells did not. The 2-chamber migration assays also revealed significantly fewer PP1 cells migrating to the lower chamber compared with the control cells (Fig. 5*e*).

To determine the activation of the Akt signaling pathway in the periostin-overexpressing and control cells, we employed western blot using a specific antibody for phosphorylated Akt. Interestingly, the phosphorylation of AKT was not observed in periostin-overexpressing cells whereas it was weakly observed in control cells (Fig. 5*f*).

Periostin has biphasic effects on the migration of pancreatic cancer cells

Because these tumor suppressive effects of periostion were inconsistent with previous studies in pancreatic cancer, we considered that the effect of periostin on the biological aggressiveness of pancreatic cancer may depend on the concentration of this protein. Therefore, we measured the concentration of periostin in the supernatant of cell lines by ELISA. The concentration of supernatants from 293T-peri cells, PP1 cells and PSC cells was approximately 150 ng/ml (Fig. 6*a*). We then examined whether the differences of the periostin concentrations affected the cell migration of Panc1 cells. As shown in Figure 6*b*, periostin at 100 ng/ml of concentration suppressed migration of Panc1 as assessed by wound healing scratch assay. In contrast, 1 μg/ml of periostin induced migration of Panc1. To elucidate the mechanism of the induction of the cell migration, the downstream signaling pathways of periostin were investigated. We treated Panc1 cells with 100 ng/ml or 1 μg/ml of periostin and assessed Akt phosphorylation by Western blotting. The phosphorylation of Akt was clearly induced when Panc1 was treated with 1 μg/ml of periostin (Fig. 6*c*, right panel),

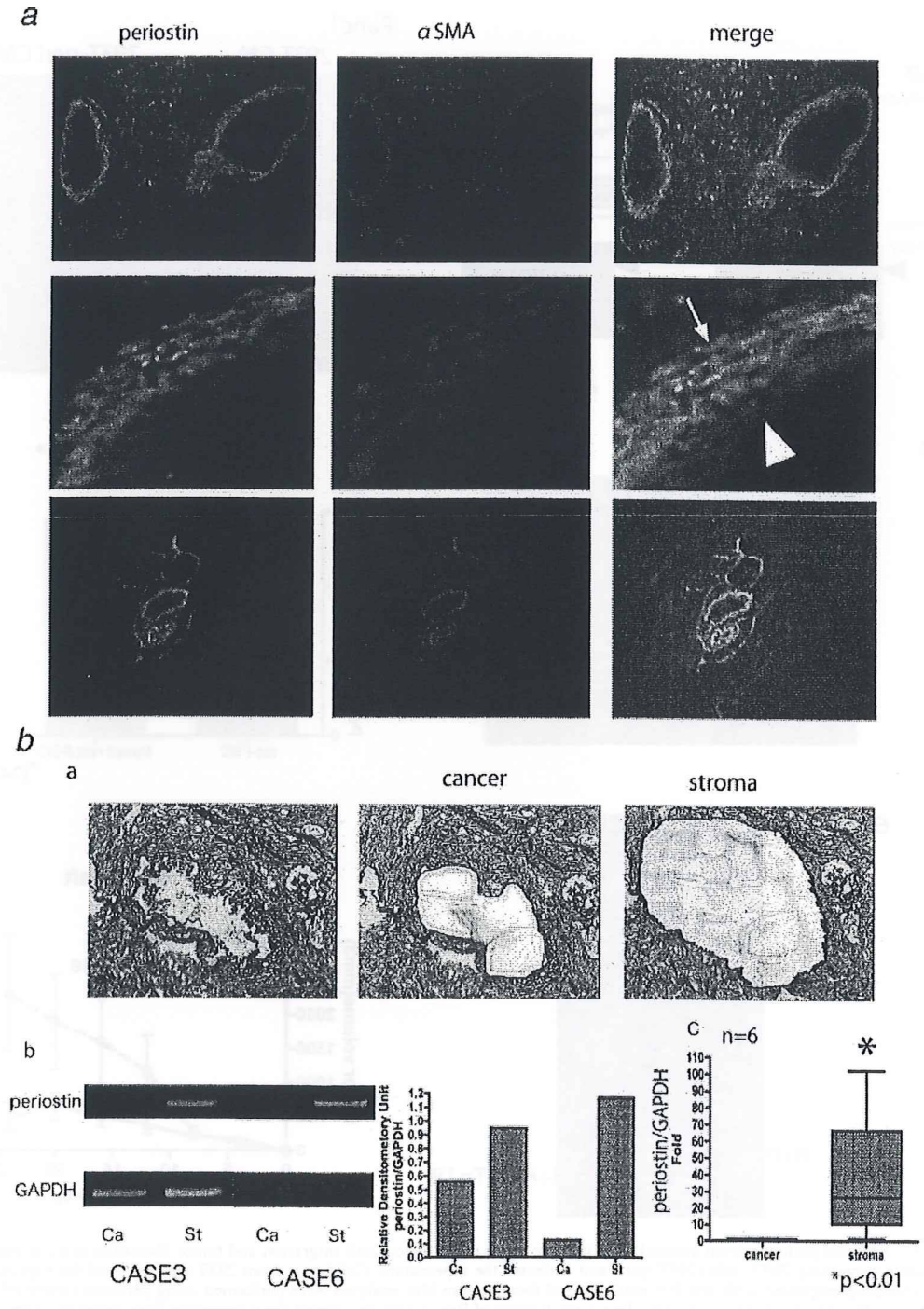

FIGURE 2 – The expression of periostin was found in stromal cells but not carcinoma cells. *a*, Double immunofluorescence staining reveals co-localization of periostin and αSMA in the pericyte and stromal area in human pancreatic cancer tissues. Periostin and αSMA expression was observed in tumor pericyte (arrow in middle panel) and stromal cells but not or background level in tumor cells (arrow head in middle panel). Coexpression of periostin and αSMA in stromal cells was frequently seen adjacent carcinoma cells (upper panel) while stromal cells around vessel infrequently demonstrated simultaneous expression these proteins (lower panel). Vessel cells showed intense coexpression of periostin and αSMA. *b*, RNA expression of periostin in microdissected cancer and stromal lesions in the pancreatic cancer. Total RNA was extracted from the microdissected lesions. Toluidine blue-stained carcinoma and stromal lesions were cut by a laser and recovered in lysis buffer (a). The real-time RT-PCR analysis clearly showed stronger expression of periostin in stromal cells than in carcinoma cells (b and c). Each sample's periostin expression level was normalized by the corresponding GAPDH expression level.

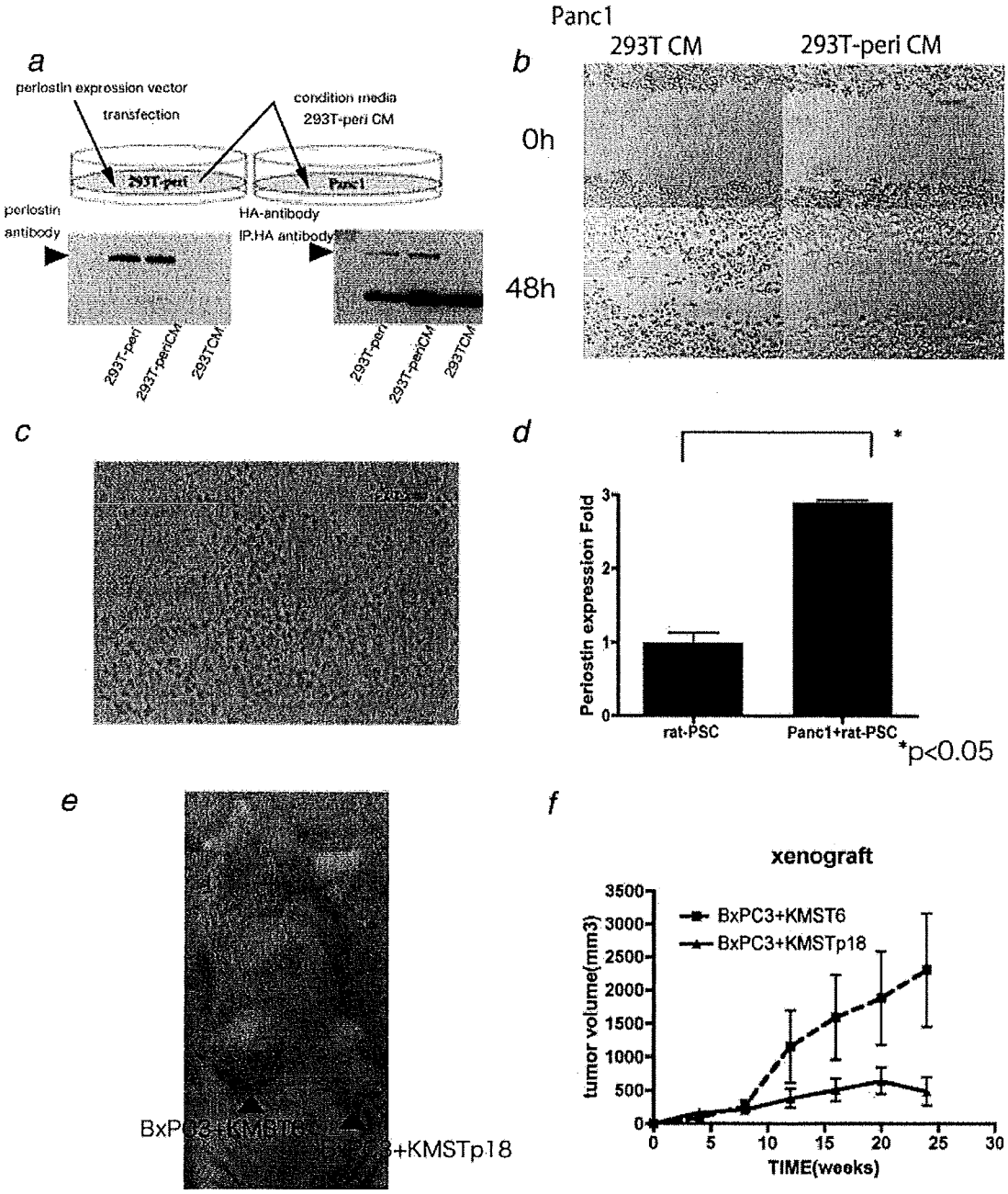

FIGURE 3 – Secreted periostin from stromal cells inhibited pancreatic cancer cell migration and tumor formation in nude mice. *a*, We established periostin expressing 293T cells (293T-peri) and collected the supernatant. Cell lysate from 293T-peri cells and the supernatant from these cells were immunoprecipitated with anti HA antibody and then western blot analyses were performed using periostin (lower left panel) and HA (lower right panel) antibody. *b*, The wound healing scratch assay of Panc1 with or without the supernatant from periostin expressing 293T cells. There were many migrated cells in the cell space after 48 hr culture with the conditioned media from control 293T, while few cells were observed in the space when Panc1 cells were cultured with media from 293-peri. *c*, Panc1 cells and rat-PSC were cocultured in contact conditions. Panc1 cells were added to monolayer of rat-PSC. Total RNA was extracted after 24 hr incubation and was subjected to real-time RT-PCR to evaluate periostin expression. The expression of periostin mRNA in the rat-PSC was significantly induced when these cells were cocultured with Panc-1 cells (*d*). *e*, BxPC3 cells together with KMST6 cells and those with periostin-overexpressing KMST6 cells (KMSTp18) were injected into the left side and the right side of the same nude mice, respectively (left panel). The tumor volume was calculated by using formula ($V = L \times W^2 \times 0.5$ (V is volume, L is length and W is width)). After 9 weeks, the mice were sacrificed. BxPC3 cells with periostin-overexpressing KMST6 cells (KMSTp18) exhibited slower growth as well as smaller tumor size in nude mice relative to those with control cells (right graph). $^*p < 0.01$.

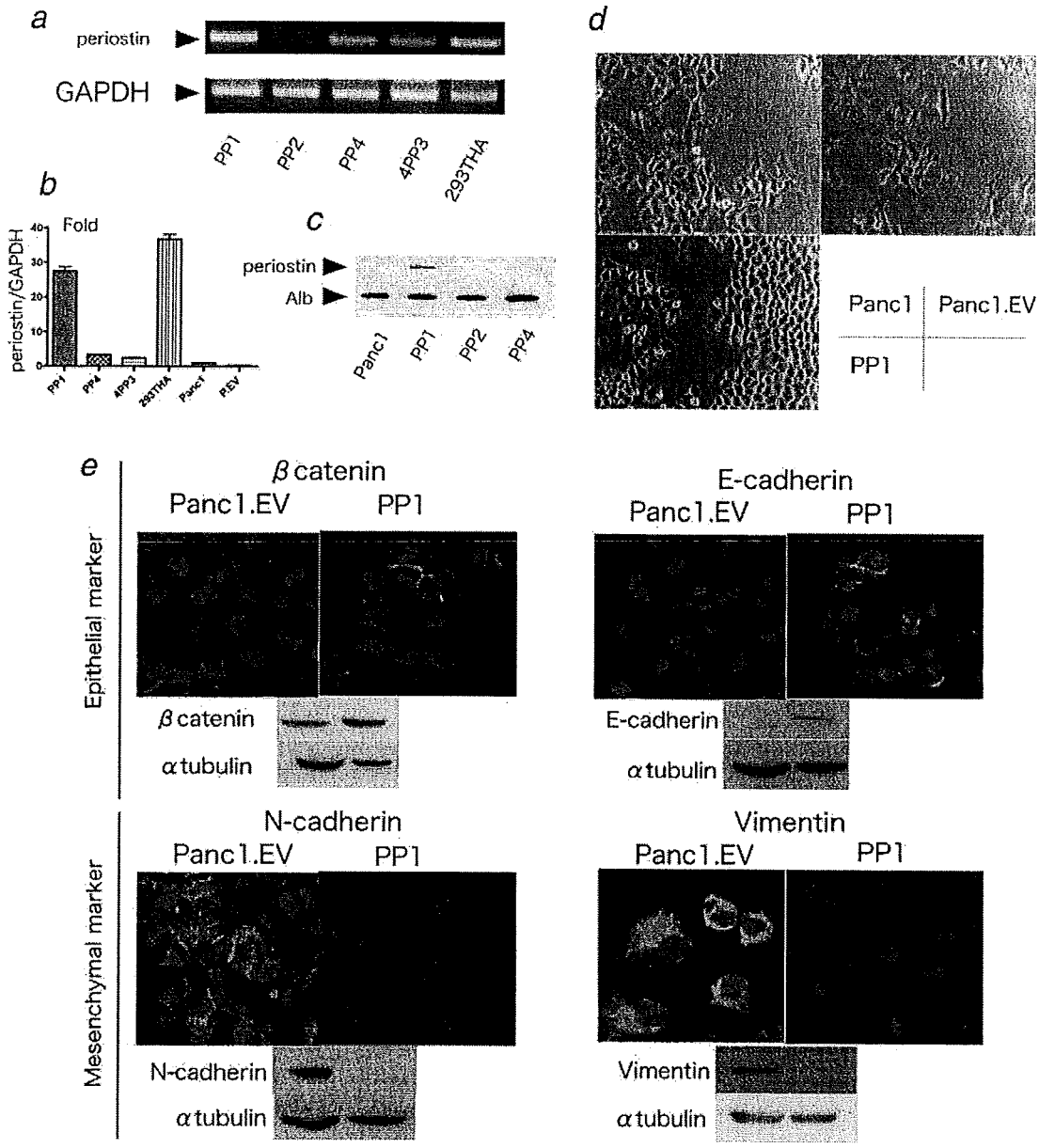

FIGURE 4 – Induced expression of periostin resulted in reversal of EMT in pancreatic cancer cells. *a*: RT-PCR analysis of periositn mRNA in several clones of periostin expression vector-transfected Panc1 and 293T cells. Specific bands for periostin were observed in all transfected cells except the PP2 clone. *b*, Real-time quantitative RT-PCR analysis of periostin mRNA level in several periostin transfected Panc1 cells and 293T cells. *c*, Forced periostin protein expression is confirmed by immunoprecipitation and Western blot analysis using anti HA antibody. *d*, Phase-contrast photographs of the Panc1 series. Panc1 and Panc1.EV cells exhibit fibroblastoid morphology, whereas PP1 cells exhibit a cuboidal epithelial morphology. *e*, Immunofluorescent staining for epithelial markers (E-cadherin and β-catenin) and mesenchymal markers (vimentin and N-cadherin) was performed in empty vector or periostin-transfected Panc1 cells. The panels under the immunofluorescent staining showed the results of Western blot analysis using the same antibody as in the upper panel and α-tubulin as loading control. Both methods clearly demonstrated that the epithelial markers were down-regulated in Panc1.EV cells but up-regulated in PP1cells. Commensurately, the mesenchymal markers were up-regulated in Panc1.EV cells, but they were down-regulated in PP1 cells.

while its phosphorylation was reduced by the treatment with 100 ng/ml of periostin compared to basal level (Fig. 6*c*, left panel). These observations clearly indicated the biphasic effect that the low concentration inhibited and the high concentration accelerated the migration of pancreatic carcinoma cells, at least in part, through the regulation of the activation of AKT.

Periostin inhibits cell growth and metastasis in nude mice

To assess whether periostin suppresses tumor growth *in vivo*, 2×10^6 of EV cells or PP1 cells were injected subcutaneously into the dorsal flank of nude mice. The tumors arising from periostin expressing cells showed significantly slower growth and were smaller compared with those of Panc1.EV (Fig. 7*a*).

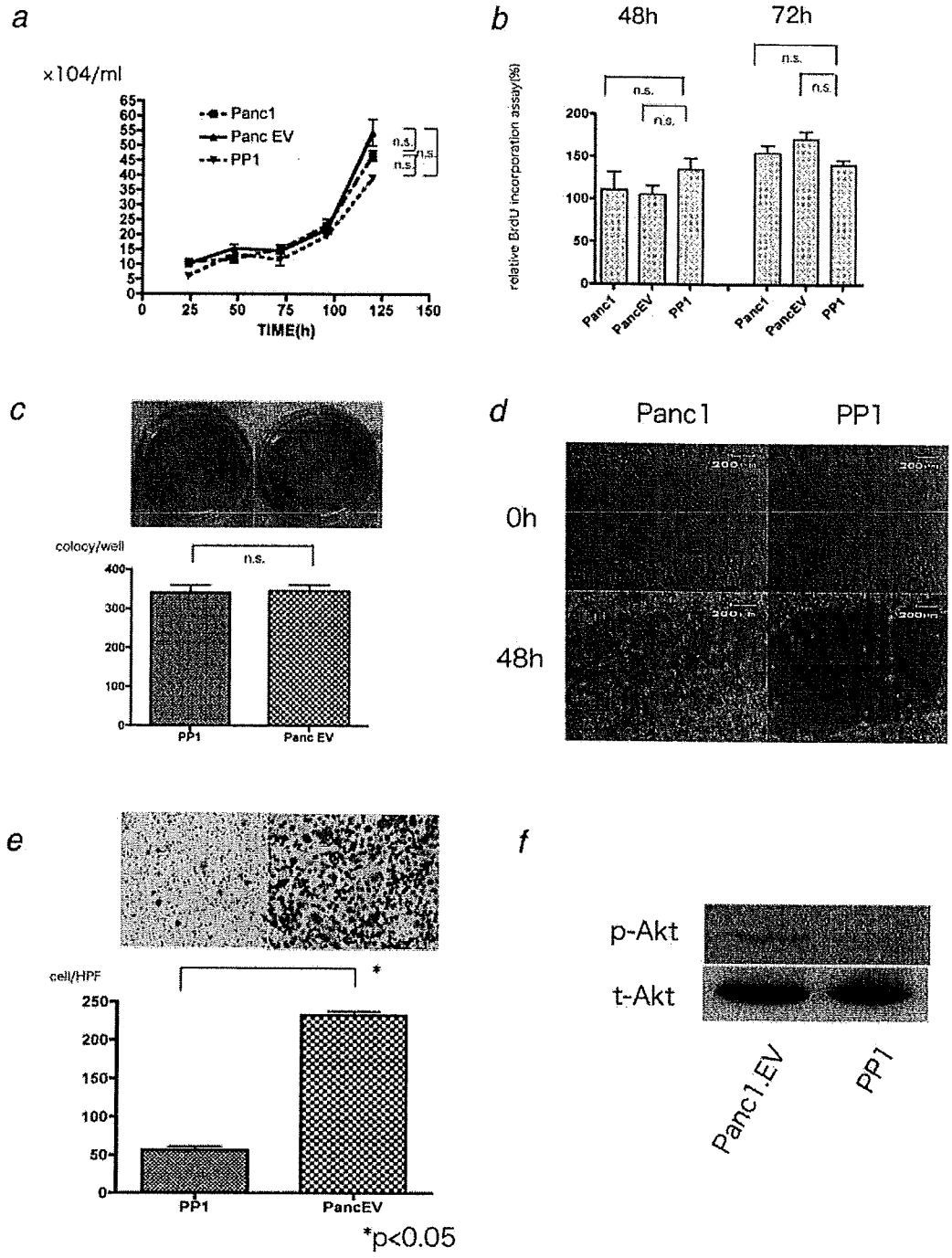

FIGURE 5 – Periostin reduced the pancreatic cancer cell migration. *a*, Panc1 and PP1 cells were seeded in a 6-well plate with normal growth media. After 1, 2, 3, 4 and 5 days, cell numbers were counted using a hemocytometer. No significant difference was observed in these cells. *b*, Panc1 and PP1 cells were seeded in 96-well plates. BrdU assay was performed after 24, 48 and 72 hr incubation using a kit according to the manufacturer's protocol. For each cell line the Proliferation Index was evaluated and the absorbance at 48 and 72 hr normalized to that at 24 hr. *c*, Equal numbers of Panc1 cells either with the periostin expressing vector (PP1) or with the control vector (Panc1.EV) were grown in soft agarose for 3 weeks. *d*, Periostin-overexpressing cells showed significantly slower migration compared with Panc1.EV. The scratched area covered by migrated cells was measured in 3 independent wells. Periostin expressing cells showed fewer migrated cells than control cells did. *e*, 2.5 × 10^4 Panc1 cells transfected with empty vector or periostin expression vector were seeded into upper chamber in serum free condition and cells that migrated toward the lower chamber, filled with media with 10% FBS as a chemoattractant, were counted after 24 hr. PancEV cells showed greater migration to the lower chamber compared to PP1 cells. *f*, Immunoblot analysis of Akt phosphorylation. The level of phosphorylated Akt was decreased in periostin-transfected cells as compared with control Panc1 cells.

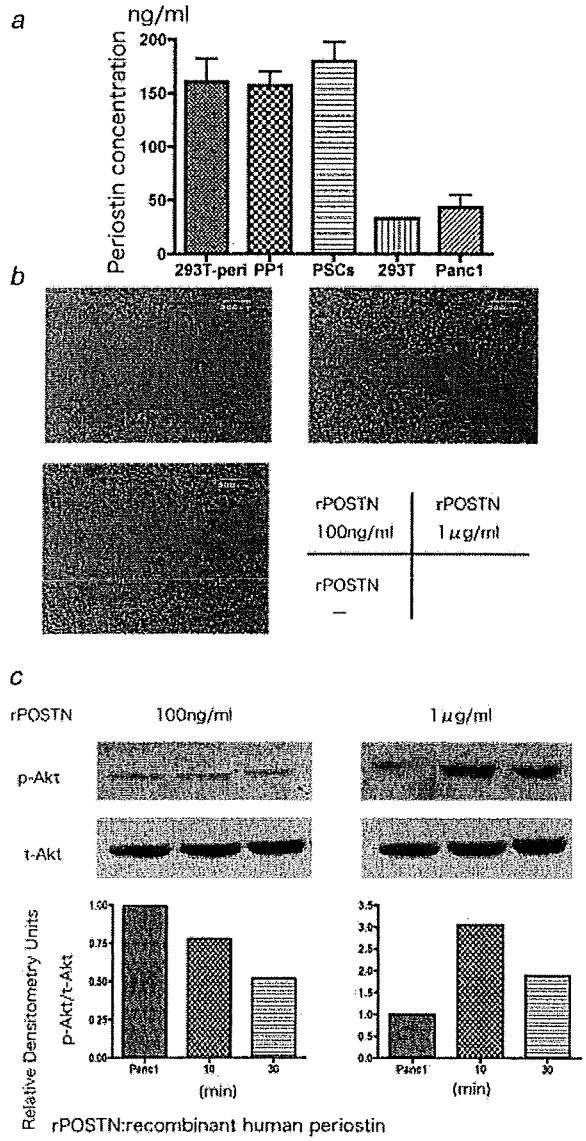

FIGURE 6 – The effects of periostin on migration are dependent on its concentration. *a*, After 24-hr incubation, periostin levels in the culture supernatant were determined by ELISA. Data shown are expressed as means + SD ($n = 3$). *b*, The wound healing scratch assay after 48 hr incubation with the various concentration of periostin (0 to 1 μg/ml). There were many migrated cells in the cell space after 48 hr culture with 1 μg/ml of human periostin, while few cells were observed in the space when Panc1 cells were cultured with 100 ng/ml of human periostin. In addition, the pancreatic carcinoma cells treated with 100 ng/ml showed fewer migrated cells in the cell space than control cells did. *c*, Western blot analyses revealed that phosphorylation of AKT was induced when Panc-1 cells were treated with 1 μg/ml of periostin (right panel) and was reduced by the treatment with 100 ng/ml of periostin. The bar graph clearly showed the reduction and induction of AKT phosphorylation by incubation with low concentration (100 ng/ml) and high concentration (1 μg/ml) of periostin, respectively.

To further evaluate if periostin overexpression affects metastasis *in vivo*, we implanted the PP1 cells and control cells (Panc1.EV) by injecting them orthotopically into the pancreatic tail of nude mice. Nine weeks after the injection, mice were sacrificed. Tumors

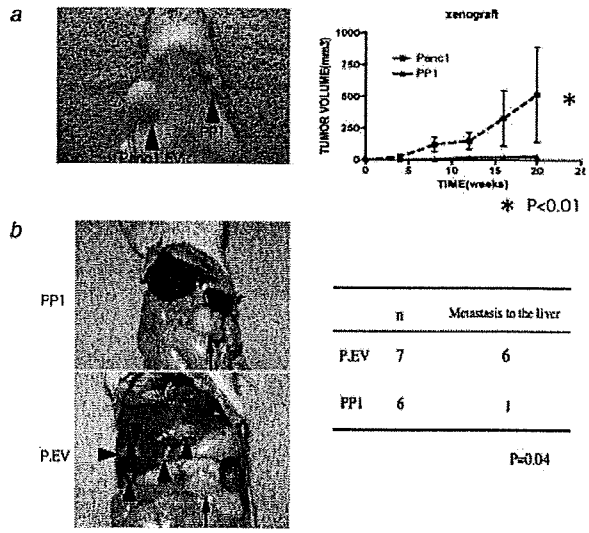

FIGURE 7 – Periostin significantly suppressed the tumor formation and the metastasis to the liver in nude mice. *a*, Two million control (Panc1.EV) cells or periostin-expressing (PP1) cells were injected subcutaneously into the left and right side of each mouse, respectively. The tumor volume was calculated by using the formula ($V = L \times W^2 \times 0.5$ (V is volume, L is length, and W is width)). After 9 weeks, the mice were sacrificed. PP1 cells exhibited slower growth as well as smaller tumor size in nude mice compared with Panc1.EV cells. $*p < 0.01$. *b*, Expression of periostin reduced metastasis of pancreatic carcinoma cells in orthotopic implantation in nude mice. Panc1.EV and PP1 cells were injected into the pancreatic tail of nude mice to examine whether the expression of periostin suppresses pancreatic cancer cell development. Seven of 7 mice with control cells and 6 of 7 mice with PP1 cells showed tumors in the pancreatic tail (arrow in B, upper panel) 9 weeks after orthotopic implantation, respectively. Six of 7 mice implanted with control cells demonstrated metastasis to the liver (arrow head in B, left lower panel), while only 1 of 6 mice implanted with PP1 cells showed metastasis to the liver.

were observed in the pancreata of both of the mice implanted with periostin-expressing cells and those with control cells. Interestingly, the periostin-expressing cells did not metastasize to the liver while multiple metastases to the liver were found in mice implanted with control cells. These findings suggested that periostin could inhibit metastasis to distant organs (Fig. 7*b*).

Discussion

Periostin contains an N-terminal secretory signal peptide, followed by a cysteine-rich domain, 4 internal homologous repeats and a C-terminal hydrophilic domain. Periostin from osteoblasts was originally identified to function as a cell adhesion molecule for preosteoblasts and precipitate in osteoblast recruitment, attachment and spreading.[16,17] Recently, proteomic and microarray profiling studies showed that periostin is up-regulated in pancreatic cancer tissues.[18–20] However, it has been demonstrated that periostin protein was mainly detected in the juxtatumoral stroma components, while the tumor cells themselves showed no immunoreactivity. Consistently, quantitative real-time RT-PCR revealed that periostin was not or very faintly expressed in pancreatic cancer cell lines, but it was strongly expressed in PSC.[12,13] In agreement with these findings, we also showed much higher levels of both periostin mRNA and protein in stromal lesions compared with those in cancer cells. In addition, PSC expressed larger amounts of periostin than cancer cells did. From these findings, we conclude that stromal cells are the major source of periostin in human pancreatic cancer tissues.

For most carcinoma, progression toward malignancy is accompanied by a loss of epithelial differentiation and a shift toward a mesenchymal phenotype. This process, referred to as "epithelial to mesenchymal transition (EMT)," intensifies the motility and invasiveness of many cell types and is often considered a prerequisite for tumor infiltration and metastasis.[3,4] Pancreatic cancer is the fourth leading cause of cancer-related deaths in the industrialized world.[21] Once pancreatic cancer is clinically evident, it rapidly develops metastatic lesions, frequently by the time of diagnosis. In addition, these tumors are usually resistant to chemotherapy and radiation.[22,23] Therefore, a new therapeutic strategy is required to improve the prognosis. We previously showed that Bone Morphogenetic Protein 4 (BMP4) induced EMT in pancreatic cancer cells with up-regulation of MSX2, and inactivation of MSX2 by siRNA suppressed EMT and inhibited the growth and metastasis of pancreatic cancer *in vivo*, suggesting that blockade of EMT could suppress tumor development. Therefore, EMT could be a candidate for a new therapeutic approach.[24,25] In the current study, induction of periostin expression to a lesser extent in pancreatic cancer cells also resulted in a reversal of the state of EMT and reduced the metastatic potential *in vivo*. Since periostin has biphasic effect, it might be one of the key genes to regulate EMT depending on the status of microenvironment.

Previous studies showed that periostin was up-regulated in various types of cancers such as the lung,[26] brain,[8] ovary,[9] breast,[27] colon[11] and oral cavity,[28,29] and its serum level was reported to be high in patients with thymoma,[30] non-small cell lung cancer[10] and breast cancer.[31] These reports suggested that periostin is involved in tumor spread, invasion and metastasis. At the molecular level, periostin activated the Akt/PKB signaling pathway[11] through $\alpha v\beta 3$[9] or $\beta 4$[12] integrins to increase cell survival. These results were entirely opposite to our findings. Erkan *et al.* have reported that periostin had biphasic effects on the Akt phosphorylation of pancreatic cancer cells. They have shown that periostin significantly decreased the Akt phosphorylation at a dose of 100 ng/ml while it increased its phosphorylation at 1 μg/ml.[13] Therefore, the present results of periostin's suppressive effects on malignant behavior of pancreatic cancer cells may have been caused by its low concentrations in the supernatants of 293T-peri cells and PP1 cells. In fact, the concentration of periostin in the supernatants from these cells was approximately 150 ng/ml which was 1/7 lower than that was used in previous study. Consistently, periostin was reported to suppress the invasiveness and metastasis of various carcinoma cells, suggesting that periostin was a tumor suppressor.[32,33] In addition, Hartel, *et al.* demonstrated that connective tissue growth factor (CTGF) was expressed dominantly in the stromal area in pancreatic cancer tissues and that patients showing high CTGF mRNA expression levels had better prognoses, indicating that desmoplastic reaction, a prominent stromal/fibrous reaction in and around tumor tissues observed in most pancreatic cancer, provides a growth disadvantage for pancreatic cancer cells.[34] This finding also supports the tumor suppressive effect of periostin because periostin was shown to be the down stream target of CTGF.[35] Although the discrepant effect of periostin for various tumors' development may be explained by its biphasic effect, it is not clear whether the desmoplastic reaction is a defense mechanism against cancer cell spreading or a growth advantage for pancreatic cancer cells.[34,36,37] Since periostin was abundantly secreted from PSC, which play a pivotal role in desmoplastic reaction,[36] and periostin has biphasic function to gain or decrease tumor aggressiveness, desmoplastic reaction may work as tumor promoter as well as tumor suppressor according to the expression level of periostin. Further study will be required to clarify the role of desmoplastic reaction and relation with periostin in pancreatic carcinoma development.

In conclusion, we demonstrated that stromal cells are the source of periostin in pancreatic cancer tissues. Pancreatic cancer cells stimulate stromal cells to secrete periostin, suggesting that cross talk between cancer cells and mesenchymal cells might further increase the periostin production in the desmoplasia. Finally, we have shown that overexpression of periostin to a lesser extent resulted in the mitigation of EMT and suppressed tumor cell metastasis, and that high concentration of periostin promoted the cell migration. These findings suggested that periostin is one of the key factors to regulate tumor-stromal interaction to accelerate or reduce tumor activity.

Acknowledgement

We thank Dr. Inoue for the periostin cDNA vector.

References

1. Hay E. An overview of epithelio-mesenchymal transformation. Acta Anat (Basel) 1995;154:8–20.
2. Thiery JP. Epithelial–mesenchymal transitions in development and pathologies. Curr Opin Cell Biol 2003;15:740–6.
3. Thiery JP. Epithelial–mesenchymal transitions in tumour progression. Nat Rev Cancer 2002;2:442–54.
4. Petersen OW, Nielsen HL, Gudjonsson T, Villadsen R, Rank F, Niebuhr E, Bissell MJ, Ronnov-Jessen L. Epithelial to mesenchymal transition in human breast cancer can provide a nonmalignant stroma. Am J Pathol 2003;162:391–402.
5. Christiansen JJ, Rajasekaran AK. Reassessing epithelial to mesenchymal transition as a prerequisite for carcinoma invasion and metastasis. Cancer Res 2006;66:8319–26.
6. Takeshita S, Kikuno R, Tezuka K, Amann E. Osteoblast-specific factor 2: cloning of putative bone adhesion protein with homology woth the insect protein fasciclin I. Biochem J 1993;294:271–8.
7. Horiuchi K, Amizuka N, Takeshita S, Takamatsu H, Katsuura M, Ozawa H, Toyama Y, Bonewald LF, Kudo A. Identification and characterization of a novel protein, periostin, with restricted expression to periosteum and periodontal ligament and increased expression by transforming growth factor beta. J Bone Miner Res 1999;14: 1239–49.
8. Sasaki H, Sato Y, Kondo S, Fukai I, Kiriyama M, Yamakawa Y, Fuji Y. Expression of the periostin mRNA level in neuroblastoma. J Pediatr Surg 2002;37:1293–7.
9. Gillan L, Matei D, Fishman DA, Gerbin CS, Karlan BY, Chang DD. Periostin secreted by epithelial ovarian carcinoma is a ligand for alpha(V)beta(3) and alpha(V)beta(5) integrins and promotes cell motility. Cancer Res 2002;62:5358–64.
10. Sasaki H, Lo KM, Chen LB, Auclair D, Nakashima Y, Moriyama S, Fukai I, Tam C, Loda M, Fujii Y. Expression of Periostin, homologous with an insect cell adhesion molecule, as a prognostic marker in non-small cell lung cancers. Jpn J Cancer Res 2001;92:869–73.
11. Bao S, Ouyang G, Bai X, Huang Z, Ma C, Liu M, Shao R, Anderson RM, Rich JN, Wang XF. Periostin potently promotes metastatic growth of colon cancer by augmenting cell survival via the Akt/PKB pathway. Cancer Cell 2004;5:329–39.
12. Baril P, Gangeswaran R, Mahon PC, Caulee K, Kocher HM, Harada T, Zhu M, Kalthoff H, Crnogorac-Jurcevic T, Lemoine NR. Periostin promotes invasiveness and resistance of pancreatic cancer cells to hypoxia-induced cell death: role of the beta4 integrin and the PI3k pathway. Oncogene 2007;26:2082–94.
13. Erkan M, Kleeff J, Gorbachevski A, Reiser C, Mitkus T, Esposito I, Giese T, Buchler MW, Giese NA, Friess H. Periostin creates a tumor-supportive microenvironment in the pancreas by sustaining fibrogenic stellate cell activity. Gastroenterology 2007;132:1447–64.
14. Bachem MG, Schneider E, Gross H, Weidenbach H, Schmid RM, Menke A, Siech M, Beger H, Grunert A, Adler G. Identification, culture, and characterization of pancreatic stellate cells in rats and humans. Gastroenterology 1998;115:421–32.
15. Masamune A, Satoh M, Kikuta K, Suzuki N, Shimosegawa T. Establishment and characterization of a rat pancreatic stellate cell line by spontaneous immortalization. World J Gastroenterol 2003;9:2751–8.
16. Skonier J, Neubauer M, Madisen L, Bennett K, Plowman GD, Purchio AF. cDNA cloning and sequence analysis of beta ig-h3, a novel gene induced in a human adenocarcinoma cell line after treatment with transforming growth factor-beta. DNA Cell Biol 1992;11:511–22.
17. LeBaron RG, Bezverkov KI, Zimber MP, Pavelec R, Skonier J, Purchio AF. Beta IG-H3, a novel secretory protein inducible by transforming growth factor-beta, is present in normal skin and promotes the adhesion and spreading of dermal fibroblasts in vitro. J Invest Dermatol 1995;104:844–9.

The American Journal of Pathology, Vol. 172, No. 4, April 2008

DOI: 10.2353/ajpath.2008.070346

Gastrointestinal, Hepatobiliary and Pancreatic Pathology

Up-Regulation of MSX2 Enhances the Malignant Phenotype and Is Associated with Twist 1 Expression in Human Pancreatic Cancer Cells

Kennichi Satoh,* Shin Hamada,* Kenji Kimura,* Atsushi Kanno,* Morihisa Hirota,* Jun Umino,* Wataru Fujibuchi,† Atsushi Masamune,* Naoki Tanaka,‡ Koh Miura,‡ Shinichi Egawa,‡ Fuyuhiko Motoi,‡ Michiaki Unno,‡ Barbara K. Vonderhaar,§ and Tooru Shimosegawa*

From the Division of Gastroenterology and the Department of Gastroenterological Surgery,‡ Tohoku University Graduate School of Medicine, Sendai City, Miyagi, Japan; Advanced Industrial Science and Technology,† Koto-ku, Tokyo, Japan; and the Mammary Biology and Tumorigenesis Laboratory,§ National Cancer Institute, National Institutes of Health, Bethesda, Maryland*

MSX2 is thought to be a regulator of organ development and a downstream target of the *ras* signaling pathway; however, little is known about the role of MSX2 in the development of pancreatic cancers, most of which harbor a K-*ras* gene mutation. Therefore, we examined whether the presence of MSX2 correlates with the malignant behavior of pancreatic cancer cells. BxPC3 pancreatic cancer cells that stably overexpress MSX2 showed a flattened and scattered morphology accompanied by a change in localization of E-cadherin and β-catenin from membrane to cytoplasm. Cell proliferation rate, cell migration, and anchorage-independent cell growth were enhanced in MSX2-expressing cells. Injection of MSX2-expressing cells into the pancreas of nude mice resulted in a significant increase in liver metastases and peritoneal disseminations compared with injection of control cells. Microarray analysis revealed a significant induction of Twist 1 expression in cells that express MSX2. When MSX2 was inactivated in pancreatic cancer cells following transfection with an MSX2-specific small interfering RNA, Twist 1 was down-regulated. Immunohistochemistry of human pancreatic carcinoma tissue revealed that MSX2 was frequently expressed in cancer cells, and that increased expression of MSX2 significantly correlated with higher tumor grade, vascular invasion, and Twist 1 expression. These data indicate that MSX2 plays a crucial role in pancreatic cancer development by inducing changes consistent with epithelial to mesenchymal transition through enhanced expression of Twist 1. *(Am J Pathol 2008, 172:926–939; DOI: 10.2353/ajpath.2008.070346)*

Homeobox-containing genes have been shown to be major regulators of morphological development of a variety of organs, and their expression levels vary during different stages of organ development.[1,2] Msx2, a member of the homeobox genes (Hox gene) family, is present in a variety of sites, including premigratory cranial neural crest, tooth, retina and lens, apical ectodermal ridge, and mammary gland.[3–9] In the development of these organs, the expression patterns of this gene suggests its active involvement in epithelial-mesenchymal interactions.

On the other hand, enhanced levels of transcripts for MSX2, the human homologue of Msx2 (HOX-8), have been shown in a variety of carcinoma cell lines of epithelial origin compared to their corresponding normal tissues. However, this enhanced expression is not found in hematopoietic tumor cells, suggesting that MSX2 plays a more important role in tumors of epithelial origin than in those of hematopoietic origin.[10] Expression of endogenous MSX2 also is up-regulated in v-Ki-*ras*-transfected NIH3T3 cells.[11] Although MSX2 itself failed to confer a transformed phenotype, antisense MSX2 cDNA as well as truncated MSX2 cDNA interfered with the transforming activities of both the v-K-*ras* and v-*raf* oncogene.[11] These findings indicated that MSX2 might be an important downstream target for the *Ras* signaling pathway. In addition, MSX2 activates cyclin D1 expression and inhibits cellular

Supported in part by grants-in-aid 17390213 and 19590745 from the Ministry of Education, Science, Sports and Culture of Japan.

Accepted for publication January 15, 2008.

Supplemental material for this article can be found on *http://ajp.amjpathol.org*.

Address reprint requests to Kennichi Satoh, Division of Gastroenterology, Tohoku University Graduate School of Medicine, 1-1, Siryo-machi, Aobaku, Sendai City, Miyagi, 980-8574, Japan. E-mail: ksatoh@mail.tains.tohoku.ac.jp.